Subsurface characterization of the Lund Sandstone– 3D model of the sandstone reservoir and evaluation of the geoenergy storage potential, SW Skåne, south Sweden

Erik Aldenius

Dissertations in Geology at Lund University,
Master's thesis, no 572
(45 hp/ECTS credits)

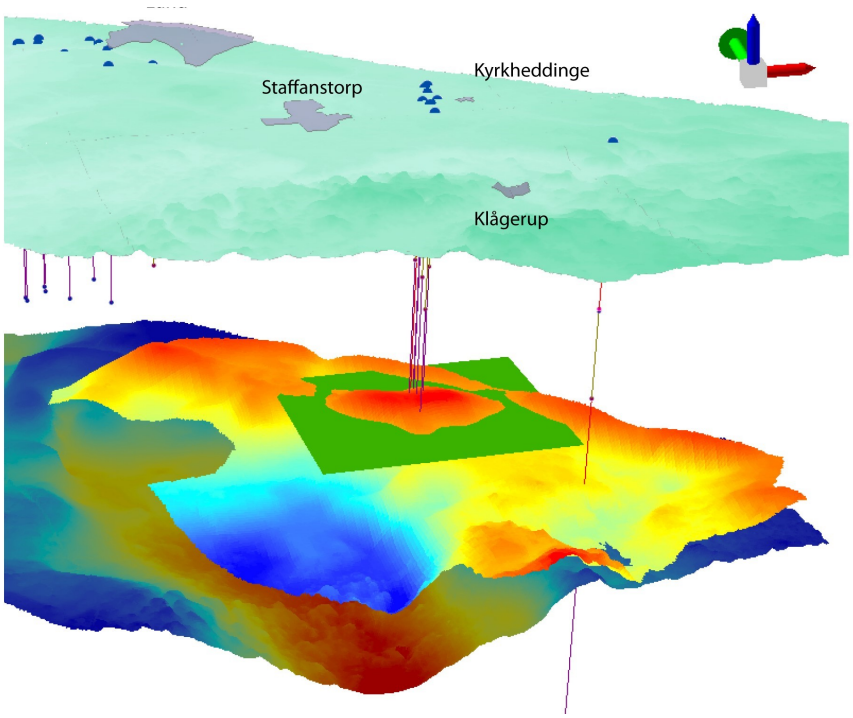

Department of Geology
Lund University
2019

Subsurface characterization of the Lund Sandstone– 3D model of the sandstone reservoir and evaluation of the geoenergy storage potential, SW Skåne, south Sweden

Master's thesis

Erik Aldenius

Department of Geology
Lund University
2019

Contents

Cover Picture: 3D model of the Lund Sandstone showing the structure in the Green Marker.

Subsurface characterization of the Lund Sandstone– 3D model of the sandstone reservoir and evaluation of the geoenergy storage potential, SW Skåne, south Sweden

Erik Aldenius

Aldenius, E., 2019: Subsurface characterization of the Lund Sandstone—3D model of the sandstone reservoir and evaluation of the geoenergy storage potential, SW Skåne, south Sweden. *Dissertations in Geology at Lund University*, No. 572, 40 pp. 45 hp (45 ECTS credits)

Abstract: In order to decrease the dependence on fossil fuels it is of paramount importance that renewable sources are used as effectively as possible. Therefore it is necessary to store excess energy when supply is higher than demand. One way to do so is by storing the energy as compressed air in a porous aquifer. The Lund Sandstone in the Kyrkheddinge area, Skåne, southern Sweden, has previously been investigated for natural gas storage. This paper tries to find a method to digitalize the analog data from these investigations to create a 3D model that can be used for further studies. The model, as well as data from the previous investigations, are used to evaluate the possibilities to utilize the Lund Sandstone for compressed air energy storage (CAES) in the Kyrkheddinge area. The well logs from these investigations and from the geothermal project outside of Lund were also evaluated to compare the geothermal energy possibilities to the Lund Geothermal Field. This was done by calculating the net sand for the wells in the two areas. The model turned out useful for evaluating possible dome structures for energy storage and could be used to determine areas and closed volumes of the structures. The possibilities for CAES in the area are slim, but one reservoir structure beneath the so-called Brown Marker, could be worth investigating further. The measured net sand is lower in the Kyrkheddinge area than in the geothermal field, but it could still be an option for a geothermal energy plant.

Keywords: Energy storage, CAES, geothermal energy, Lund Sandstone, renewable energy, geoenergy

Supervisor(s): Mikael Erlström

Erik Aldenius, Department of Geology, Lund University, Sölvegatan 12, SE-223 62 Lund, Sweden. E-mail: erikaldenius@gmail.com

Karakterisering av Lundasandstenen—3D model av sandstensreservoaren och utvärdering av lagringspotentialen av geoenergi, sydvästra Skåne, södra Sverige

Erik Aldenius

Aldenius, E., 2019: Karakterisering av Lundasandstenen—3D modell av sandstensreservoaren och utvärdering av lagringspotentialen av geoenergi, sydvästra Skåne, södra Sverige. *Examensarbeten i geologi vid Lunds universitet*, Nr. 572, 40 sid. 45 hp.

Sammanfattning: För att minska vårt beroende av fossila bränslen så är det viktigt att de förnybara energikällorna används så effektivt som möjligt. För att göra detta krävs det att vi förvarar överskottsenergi när efterfrågan är lägre än tillgångarna. Ett sätt att göra detta är att förvara energin som komprimerad luft i en porös akvifär. Lundasandstenen i Kyrkheddingeområdet har tidigare blivit undersökt för möjligheten at förvara naturgas. Det här arbetet utforskar möjligheten att digitalisera den analoga datan från dessa undersökningar för att skapa en 3D modell som kan användas i ytterligare studier. Modellen, samt data från de tidigare undersökningarna, används för att undersöka möjligheten att använda Lundasandstenen för lagring av komprimerad luft (CAES) i Kyrkheddingeområdet. Borrloggarna från dessa undersökningar och från geotermiprojektet utanför Lund undersöktes också för att utvärdera möjligheterna för geotermi jämfört med Lundafältet. Detta gjordes genom att beräkna nettosand i borrhålen i båda områdena. Modellen visade sig vara användbar för att utvärdera möjliga domstrukturer som kan användas för energilagring och kunde användas för att beräkna strukturernas areor och volymer. Den kan vara användbar för liknande studier. Möjligheterna för energilagring i form av komprimerad luft är små, men en reservoar under den seismiska markören `Brown Marker', kan vara värd att undersöka. Den uppmätta nettosanden är lägre i Kyrkheddingeområdet än i Lundafältet, men kan ändå vara ett alternativ.

Nyckelord: geoenergi, geotermi, energilagring, Lundasandstenen, förnybar energi,

Handledare: Mikael Erlström

Ämnesinriktning: Berggrundsgeologi

Erik Aldenius, Geologiska institutionen , Lund University, Sölvegatan 12, SE-223 62 Lund, Sweden. E-mail: erikaldenius@gmail.com

1 Introduction

As energy consumption increases and more focus is being put on renewable energy sources we are faced with new challenges regarding assessment of the geothermal resources (Li et al. 2018). The efficiency of renewable sources such as wind and solar power vary over time and the generated energy does not always match the demand (Li et al. 2018). To increase the use of these renewable sources there is a need that they are stable over time to match the demand, thus increasing their degree of accessibility (Mouli-Castillo et al. 2019). One way of doing this is to create buffer capacities in the distribution systems where energy storage of various kinds is considered a way forward. One way of storage is utilizing deep sandstone reservoirs. Storage of natural gas in deep reservoirs is an established method in many countries, i.e. in the Stenlille area in Denmark there is a major storage facility utilizing the porous and permeable sandstones of the Lower Jurassic Gassum Formation. Similarly, in the sedimentary subsurface bedrock in Germany there are several storage facilities for natural gas. Deep saline aquifers are also considered main alternatives for storage of CO_2 (Wang et al. 2016). In Sweden, suitable sandstone reservoirs are merely found in the sedimentary bedrock on Gotland and in south-west Skåne. The sedimentary succession in south-west Skåne includes a series of potential sandstone units of Mesozoic age, which might prove suitable both for extraction of geothermal heat and for energy storage. One of these is the Upper Cretaceous Lund Sandstone which presently is used for extraction of geothermal heat for the city of Lund (Aldenius 2017). The sandstone is considered one of the most potential storage reservoirs based on the vast knowledge on the reservoir hydraulic properties from more than 30 years of production and injection of geothermal water in the Lund geothermal plant. Besides this data there is also considerable amounts of information from a pre-investigation project regarding storage of natural gas in the Kyrkheddinge area south-east of Lund (Lindblom & Svenssson 1985). These prerequisites have been used in the following study. The main task has been to compile existing analogue data into digital format with the aim to create 3D-models for the reservoir units and estimate the reservoir volume for closed parts of the formation. In combination with existing petrophysical data an assessment of the storage capacity is performed. Another purpose of the study has been to perform a methodology study on how older analogue and raster data can be used in the process of constructing a 3D model of the Lund Sandstone reservoir.

2 The area of investigation

The Lund Sandstone is found along the north-east margin of the Danish Basin in Skåne (fig. 1). The subsurface outline is known from regional seismic surveys performed by OPAB during the 1970-s. The performed investigation has incorporated this information into a regional digital 3D model, which shows the top and base of the Lund Sandstone. The outline of this area is shown in fig. 2. Focus has, however, been put on a compilation and modeling of a 36.5 km^2 large area south-east of Lund, at Kyrkheddinge (fig. 3). Information about the Lund Sandstone has also been obtained from the Lund geothermal field.

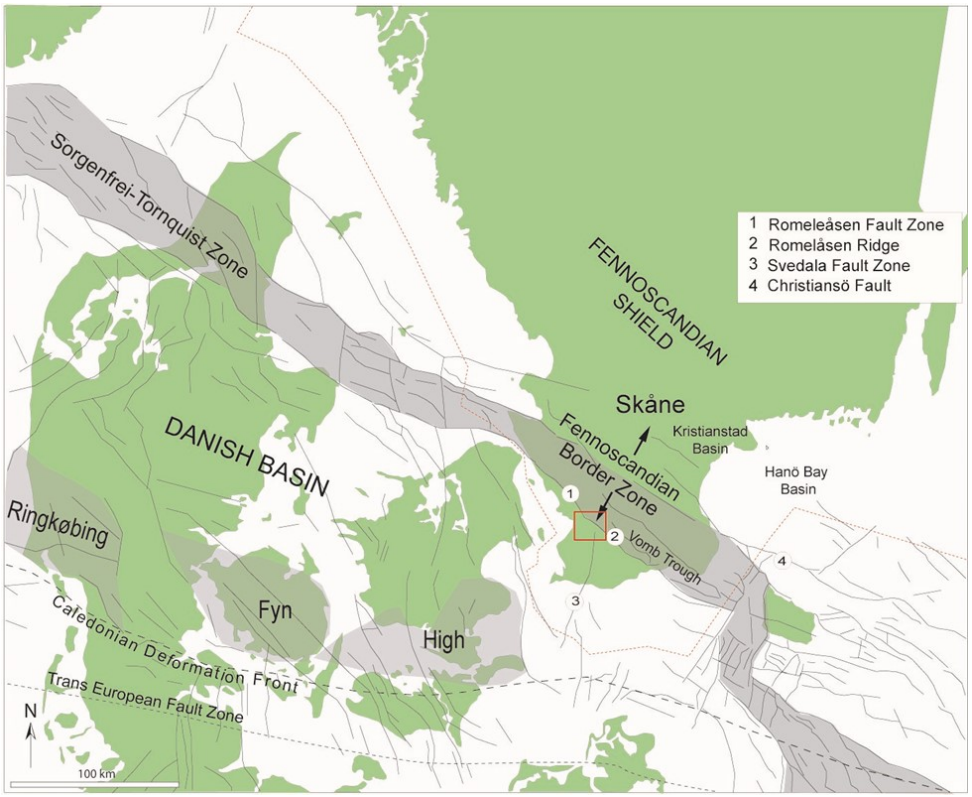

Fig. 1. Map of the tectonic structures in Skåne and Denmark. The studied area is shown as a red framed area. It is situated at the margins of the Danish Basin on the south side of the Sorgenfrei-Tornquist Zone (modified from Erlström 2009).

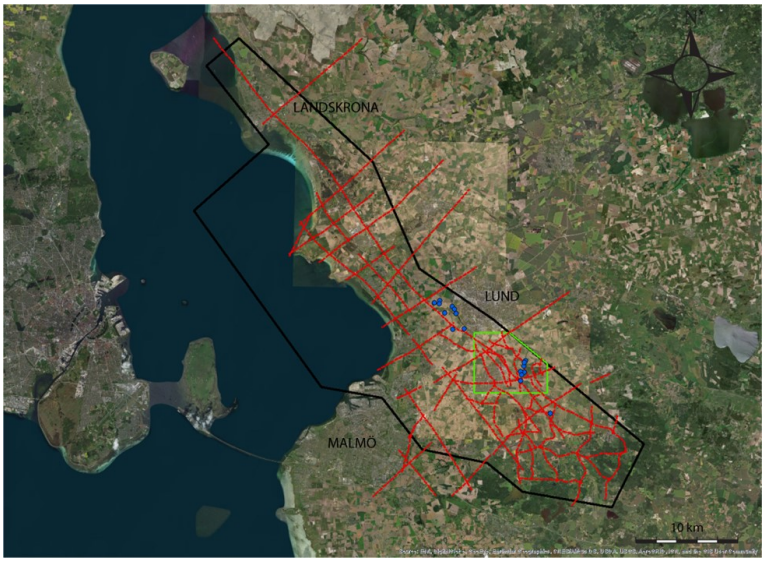

Fig. 2. Aerial photo of western Skåne. The investigated area is marked with black borders. This area is 700 km^2. The green frame marks the Kyrkheddinge area in which the detailed modeling has been performed. This area is 36.5 km^2 (fig. 3). The blue filled circles show the locations of the studied wells and the red lines represent the seismic lines that the isochron maps are based on.

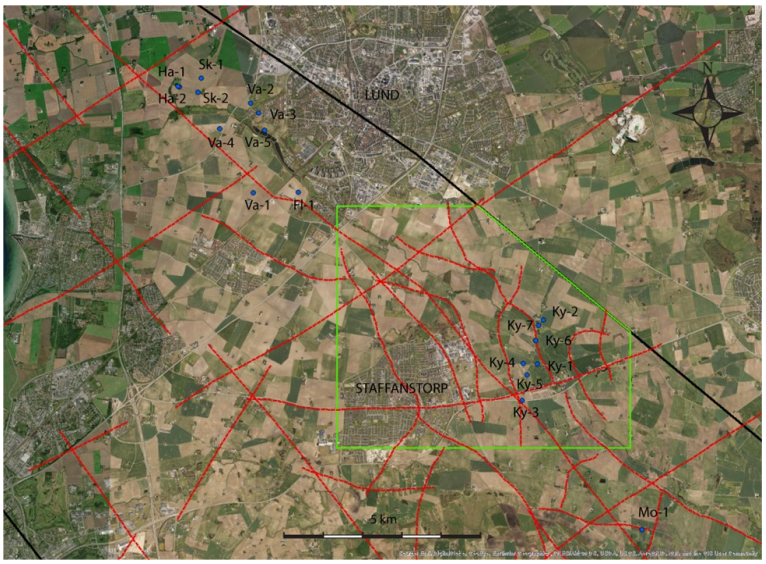

Fig. 3. Close up of the Kyrkheddinge study area (in green). Blue filled circles are the studied wells. Red lines are the seismic lines which the isochron maps are based on. The wells included in the Lund geothermal field are shown in the upper left area outside the town of Lund.

2.1 The Kyrkheddinge area

During the end of the 1970s there was an increasing interest in finding suitable sites for aquifer storage of natural gas in Skåne. The launched extensive investigation program that took place 1977–1985 is summarized by Lindblom & Svenssson (1985). Site selection investigations were done by Swedish Geological Survey (SGU) 1977–1982 and the first investigations was mainly based on seismic and well data from hydrocarbon explorations in Skåne done by Oljeprospektering AB (OPAB). In 1980 and 1982 new seismic investigations were made to add to the data available. The French company Sofregaz evaluated the SGU investigations and found the Kyrkheddinge structure, situated on the south-west side of the Romeleåsen Horst, to be most suitable for storage out of five different structures found. In 1982 three slimholes were drilled, Kyrkheddinge -1, -2, and -3 (Ky-1, Ky-2, Ky-3), targeting the Lund Sandstone. Additional seismic lines were measured in 1983 as well as a drilling of conventional sized well, Kyrkheddinge-4 (Ky-4). The most interesting find was a structure corresponding to the seismic horizon called the Green Marker, which is a 6–26 m thick cap rock of argillaceous limestone (fig. 4). Beneath this lies a 40 m thick porous sandstone aquifer called Sand B. The seismic investigations show a possible 4.5 km^2 convex structure at around 750 m depth that could be a possible storage reservoir. The seismic investigations showed that the Sand B and associated caprock showed the most promising properties and structure regarding its suitability for storage of natural gas (Lindblom & Svenssson 1985). Three more slim-hole investigation wells were therefore subsequently drilled by Microdrill in 1984, i.e. Kyrkheddinge-5, -6, and -7 (Ky-5, Ky-6 and Ky-7). The well data from these showed that the Green Marker structure, that was visualized in the seismic data as an anticlinal structure, was less significant than expected, and that it also flattens out to the north-east. This rendered that the closed potential reservoir volume was not enough. Due to this the aquifer was thought to be unsuitable for gas storage and in 1985 the Swedegas storage exploration project was shut down (Lindblom & Svenssson 1985). Other possible reservoirs levels in the area are described by Hagconsult AB (1983). They identified six different aquifers, Sand A–G, with Sand A being the deepest lying one. Sand G is the shallowest aquifer at less than 600 m depth and with a cap

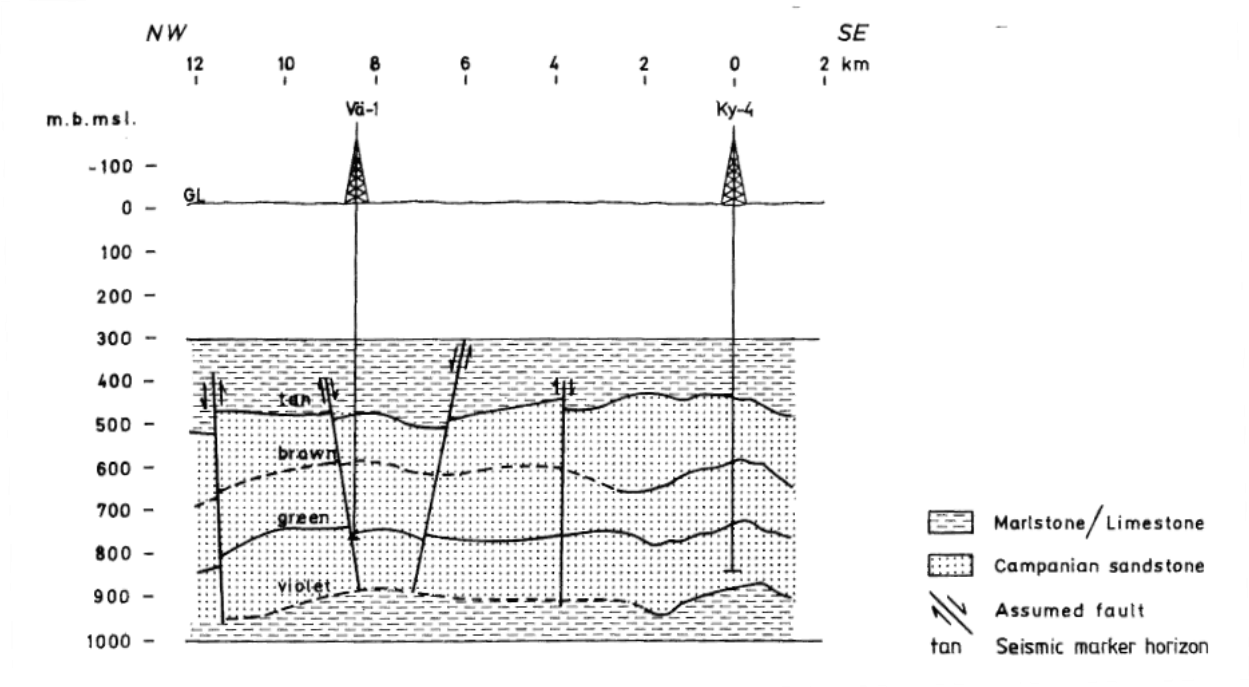

Fig. 4. Marker horizons along a schematic cross-section between Vä-1 in the Lund geothermal field and Ky-4 in the Kyrkheddinge field showing possible anticlinal structures in the Brown and Green Marker by the Ky-4 well (Andersson et al. 1984).

rock just 2 m in thickness. It is thought to correspond to the seismic lines called the Brown Marker and is less well studied than Sand B.

2.2 The Lund geothermal field

The data from OPAB was also used by the Division of Engineering Geology, LTH, at Lund University in their work on assessing the geothermal potential of the Mesozoic sandstone reservoirs in south-west Skåne (Alm & Bjelm 1995). Their investigations, that started in 1982, focused on the Lund Sandstone, and in 1985 the geothermal plant started its operations in Lund (Bjelm & Lindeberg 1994). During the initial phase of investigation two test wells were drilled west of Lund, i.e. Flackarp-1 and Värpinge-1 (Fl-1 and Vä-1) (Lunds Tekniska Högskola 1984). These wells gave valuable information regarding the general reservoir properties of the Lund Sandstone, such as temperature, net sand and hydraulic properties. Based on the outcome of these two exploration wells ten additional wells were drilled and incorporated in the Lund geothermal plant. All wells were investigated using various logging methods including natural gamma logs, which have been used in the overall assessment of the reservoir included in this study. The Lund geothermal system has now been running for more than 30 years and is still a significant component in the Lund district heating system. An evaluation of the production history is presented by Aldenius (2017).

3 Materials and methods

3.1 Well data

During the natural gas storage investigations by Swedegas AB 1978–1985 seven wells were drilled in the Kyrkheddinge area: Ky-1–Ky-7. In this study wire-line logs from these seven wells, the eleven wells in the Lund Geothermal field, Hansagården 1–2 (Ha-1 and Ha-2), Skälsåker 1–2 (Sk-1 and Sk-2), Värpinge 1-6 (Vä-1 – Vä-6) and Flackarp 1 (Fl-1), and one well south of the Kyrkheddinge area, Mossheddinge 1 (Mo-1), were used. Logs were available for all wells except for Vä-1. The Natural gamma logs were used for all wells to identify the sandstone beds. The well data was evaluated together with the reports from the natural gas explorations in the area and supported by the well-evaluations presented by Erlström (1990).

3.2 Seismic data

The existing seismic data set consists of data from several campaigns. The first one was a regional study performed by OPAB and in phase 3 of the natural gas storage investigations lines were added in Vellinge and Mossheddinge (Kumpas 1981). Five areas were selected for additional seismic investigations in phase 4, Kyrkheddinge, Klågerup, Anderslöv, Mossheddinge-Sturup, and two lines in the Vomb Trough (Larsson & Kumpas 1982). During phase 5 three new seismic lines were carried out in Kyrkheddinge where two (M5X and M5Y) were done in the north-north-east region and the last one (M5Z) covered the top of the structure (Larsson 1982). Seismic investigations were also made in Törringe and Skurup during this time (Sofregaz 1982). These were all done with the mini-sosie technique (Barbier et al. 1976). In phase 8 extensive seismic investigations were carried out in the Kyrkheddinge area with shot-hole technique to improve on the data quality (lines S1–S4) (fig. 5) (Lindblom & Svenssson 1985). During the early investigations the seismic data had been evaluated and a few significant levels were recognized. The Tan Marker was recognized as the top of the Lund Sandstone, the Orange Marker is a layer slightly below the top, the Brown Marker is related to a dense cap rock in the sandstone.

The Green Marker is another significant cap rock and the Yellow Marker is related to the base of the Lund Sandstone (table 1). Isochron maps are available for these markers showing the depth in two-way travel time (TWT) compiled by SGU and Pipeline Engineering for the Swedegas project (fig. 6) (Lindblom & Svenssson 1985). The Orange, Brown, Green and Yellow markers were first mentioned by Cherns & Larsson (1980) and the Tan Marker was added by Larsson & Kumpas (1982). The definitions of the markers were revised and changed by PLE (1983). The Tan Marker is only mapped in the Kyrkheddinge area whereas the Yellow Marker is mapped from north of Landskrona along the south-west side of the Romeleåsen Horst down to Mossheddinge south of Lund.

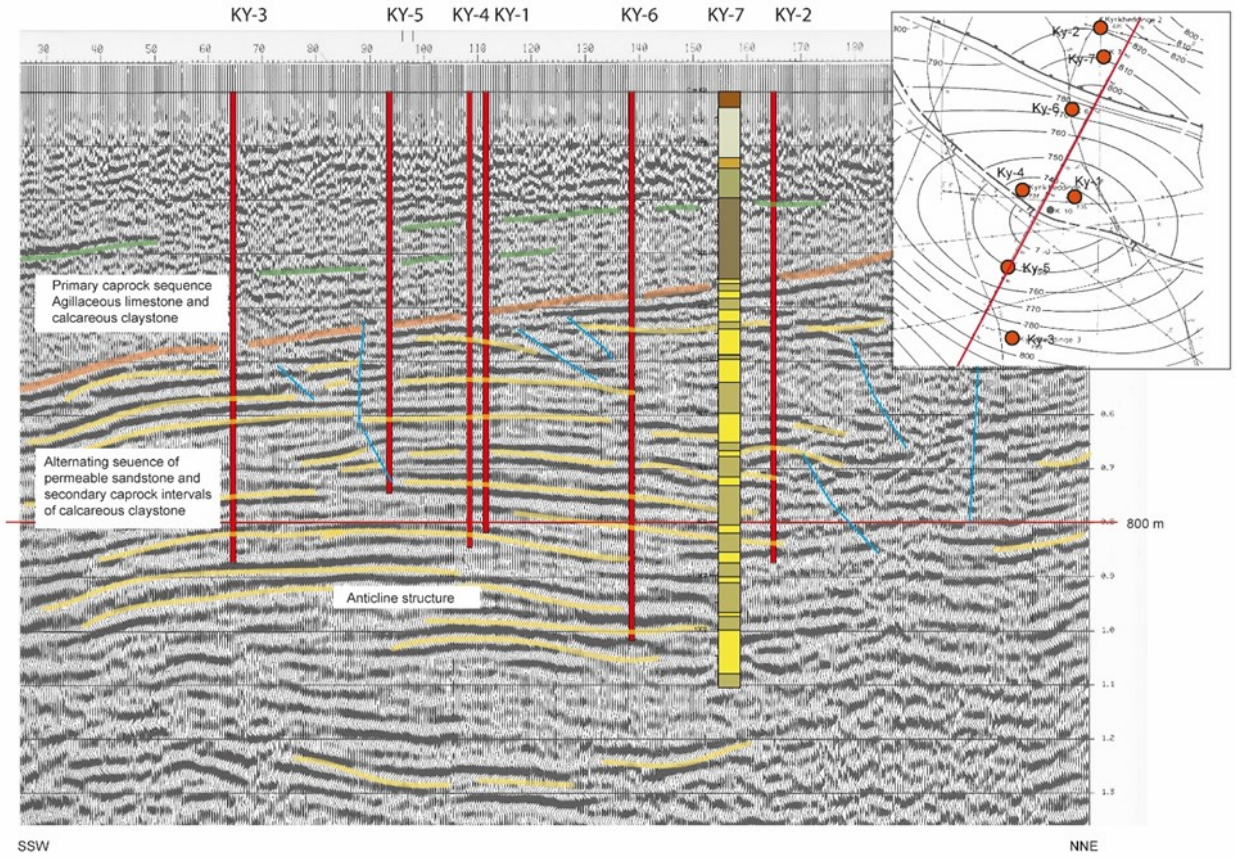

Fig. 5. Example of the seismic signature of the Lund Sandstone in the Kyrkheddinge area. Line S4 with allocated wells along the line. Sandstone dominated intervals are marked in yellow (Bjelm et al. 2014).

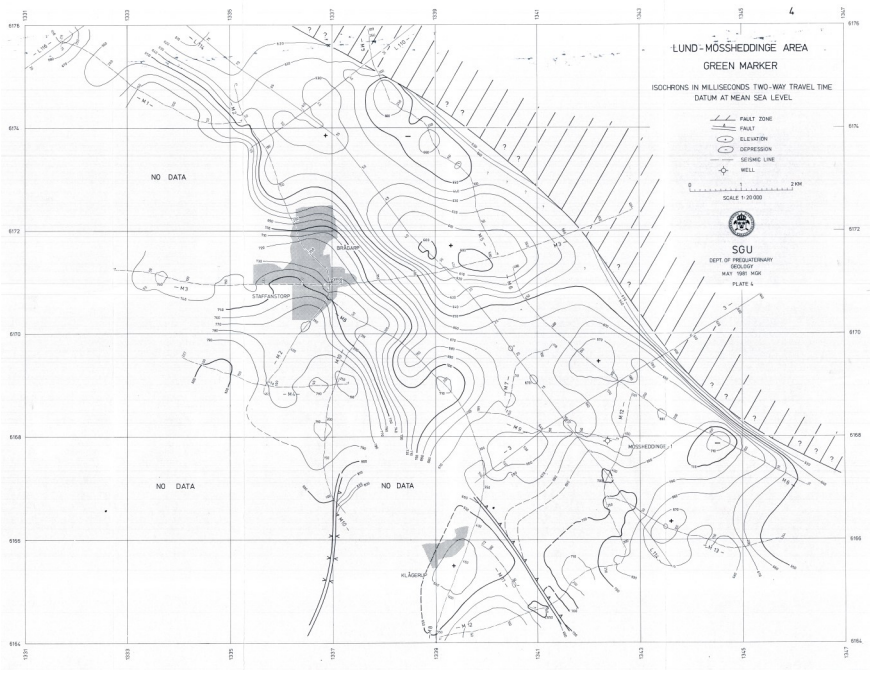

Fig. 6. The isochron map of the Green Marker in the Lund-Mossheddinge area (the other isochron maps are shown in the appendix). These maps are based on the seismic data and show the depth to the marker in TWT (two-way travel time). These isochron maps are the basis for the 3D model (SGU 1981).

Table 1. The different markers that were mapped as major stratigraphic boundaries in the Lund Sandstone, based on seismic investigations.

Marker	*Lithostratigraphic correlation*
Tan	Top of the Lund Sandstone
Orange	Base of a sandstone close to the Tan Marker
Brown	Caprock G
Green	Base of caprock B
Yellow	Bottom of the Lund Sandstone

3.3 Additional data

Beside the borehole information and seismic survey, data from petrophysical analyzes on core material from the Kyrkheddinge wells have been used in this study. These data are gathered from various unpublished reports found in the archives at the Geological Survey of Sweden. In addition, the geological interpretations reported from the natural gas storage investigations and the interpretations presented in Erlström (1990) have been taken into consideration. Elevation data from Lantmäteriet has been used as references for the ground level used for 3D-modelling evaluation.

3.4 Digital modelling

Before the 3D-model could be created the data were handled in ArcMap as maps in 2D. For the 3D modelling the extension program ArcScene was used. Refining of figures was done in Adobe Illustrator.

The workflow for creating the model is shown in fig. 7. The first step in creating the model is digitalizing the existing isochron maps. The maps were scanned and transferred to ArcMap where they were fitted to the SWEREF99 grid and the isolines for the various stratigraphic marker horizons traced and a line shape file was created. The isolines were recalculated from Two Way Travel (TWT), time in seconds, to metric depths by using the well data. First the average bedrock velocities were calculated for each marker by correlating the TWT from the isochron maps with the depths from the well data, using this equation:

$$v = \frac{d}{TWT/2}$$

Where v is the velocity, d is the depth, TWT is two-way travel time. Since the bedrock is heterogenous the velocity varies between sites so an average between all the well velocities was used. Since the top of the Lund Sandstone (Tan Marker) is only mapped in the Kyrkheddinge area the wells Ky-1–7 were used to calculate the velocity. The same velocity was used for the Orange Marker since it is very close to the Tan Marker and there is no well data available for it. The velocity for the base of the formation (Yellow Marker) was calculated from the wells Mo-1 and Ky-7 since these are the only ones that penetrate the complete Lund Sandstone. The velocity for cap rock B (Green Marker) and cap rock G (Brown Marker) is based on the depths specified from the well Ky-4. The isolines were then recalculated into metric depth with the help of the calculated velocities, using this equation:

$$d = \frac{TWT \times v}{2}$$

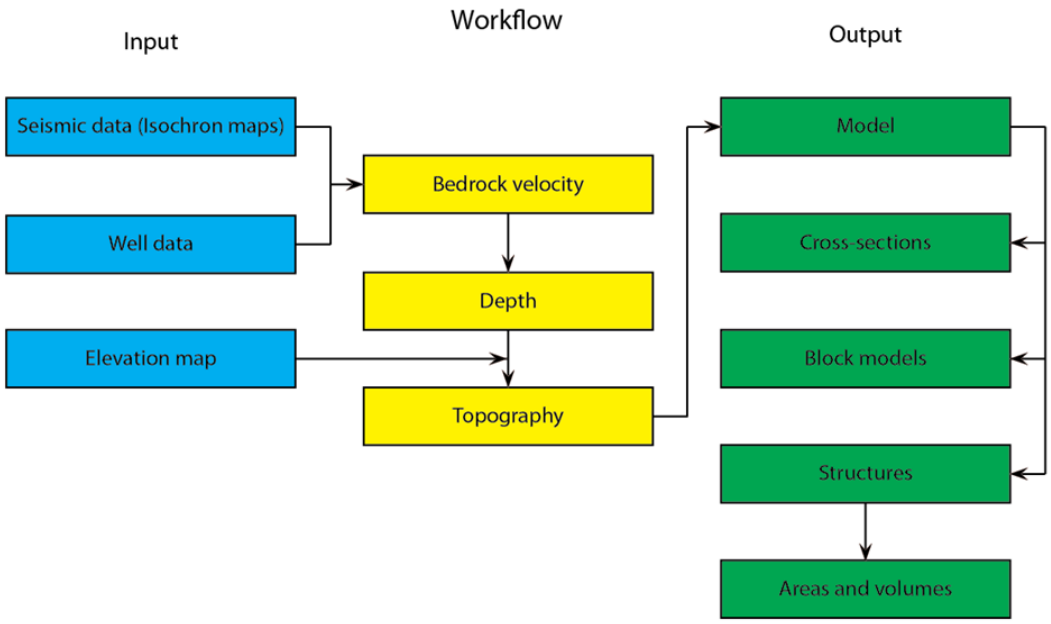

Fig. 7. Workflow for creating a 3D model in ArcScene. The first steps are done in ArcMap. The seismic data combined with well data gives bedrock velocity and can then be used to calculate the depth. Together with an elevation map over the area the isochron maps can then be used to map out the depth. Once topography maps are created for each layer these can be transferred to ArcScene where they can be displayed in 3D at the correct depth as raster files. These have good details and can be used to find structures in the formation, such as anticline structures, and areas and volumes can be calculated in great detail. Block models can also be created as well as cross-sections, but these have less details and are not used for this study.

The isolines were then turned into a raster surface and combined with the ground elevation raster from Lantmäteriet to correct the depth in relation to the ground level. All the surfaces were then transferred to ArcScene where they could be presented as 3D surface. The raster files can also be turned into TIN files (triangular irregular networks) which makes it possible to make blocks of the formation to be presented as cross-sections.

The closure depths of the dome structures that were recognized in the Brown and Green markers were checked by creating a horizontal surface which could be used to check at which depth the structure was open (fig. 14–16). The structures were then turned into their own raster surface and in ArcScene their area and volume could be calculated with the Surface Volume 3D analysist tool.

3.5 Assessment model for energy storage

The possibilities to use the Kyrkheddinge aquifer for Compressed Air Storage (CAES) is evaluated with the help of criteria suggested by Succar & Williams (2008) (table 2). Besides the suggested criteria other important data related to CAES were compiled based on Sopher et al. (2019). The data used to do the evaluations come from the natural gas storage investigations and the model created for this thesis.

The permeability needs to be high enough to have good flow rate in the aquifer and should at least be around 300 mD for successful CAES operations together with a porosity preferably above 13 % to have enough pore space (Succar & Williams 2008). For this thesis these values are taken from the Natural Gas storage investigations and are derived from core samples and well logging. Total reservoir volume (V_R/V_S) is the volume of pore space above the spill point (V_R) compared to the size needed for CAES operation (V_S) and should be close to 1, too small and operation is not possible, too large and it drives up the cost of the plant (Succar & Williams 2008). Since no plant is planned in the study area comparison is made to a large scale CAES plant that is under construction; the Norton plant in the USA. Total closure rating (*h/H*) is the proportion of the reservoir which is above the spill point where *h* is the height of the reservoir above the spill point and *H* is the total height of the reservoir for any given point (Succar & Williams 2008). Here *h* is derived from the volume and area given by the model (V/A=h) to give an average height of the reservoir above the spill point. H is taken from Hagconsult AB (1983). The depth and pressure is based on the integrity of the caprock and limits on the machinery and is based off of a study done in 1982, which means that higher pressures could be possible with newer machinery (Succar & Williams 2008). Pressure tests were

Table 2. Ranking criteria for CAES taken from Succar & Williams (2008). These are used to evaluate how suitable a porous aquifer is for compressed air energy storage. A higher score means a better fit for storage, but a score of 1 in one of these criteria means it cannot be used as a storage as it lacks a vital property.

Score	*1*	*2*	*3*	*4*	*5*
Score Interpretation	Unsatisfactory	Poor	Satisfactory	Good	Excellent
Permeability (mD)	<100	100–200	200–300	300–500	>500
Porosity (%)	<7	7-10	10–13	13–16	>16
Total Reservoir Volume (V_R/V_S)	<0.5		0.5–0.8 or >3	0.8–1.0 or 1.2–3.0	1.0–1.2
Total Closure Rating (h/H)	<0.5		0.5–0.75	0.75–0.95	0.95–1.0
Depth to Top of Reservoir (m)	<137 or >760	140–170	170–260 or 670–760	260–430 or 550–670	430–550
Reservoir Pressure (bar)	<13 or >69	13–15	15–23 or 61–69	23–39 or 50–61	39–50
Type of Reservoir	Highly discontinuous	Moderately vulgar limestone & dolomite	Reefs, highly vulgar limestone & dolomite	Channel sandstones	Blanket sands
Residual Hydrocarbons (%)	>5%		1–5%		<1%
Cap rock leakage	Leakage evident	No data available		Pumping tests show no leakage	
Cap rock Permeability (mD)			$>10^{-5}$	$<10^{-5}$	
Cap rock Threshold Pressure (bar)			21–55	<55	
Cap rock Thickness			<6	>6	

performed during the natural gas storage investigations and the depth is based on the model. The type of reservoir affects the flow through the aquifer, blanket sands are the best alternative whereas a highly discontinuous reservoir would not work as it would limit the flow rate (Succar & Williams 2008). One problem that can appear in porous aquifers is residual hydrocarbons, which can create compounds that reduce permeability as well as a risk for flammability when introduced to high pressure air. This is mainly a problem when the reservoir is located in a depleted oil or gas reservoir (Succar & Williams 2008) and has not been included in the chemical testing done. The last important thing in evaluating a reservoir for CAES operations is the cap rock properties. In order to know if the cap rock can hold air under high pressures cap rock thickness and permeability has to be known and cap rock leakage and cap rock threshold pressure, at which pressure leakage starts, needs to be tested (Succar & Williams 2008). The thickness and permeability were investigated during natural gas storage investigation with cores and well logs, but no tests have been done on leakage and threshold pressure in the area.

Other important properties for CAES operations are, area of closure and gross rock volume which are calculated from the model. In order to calculate pore volume, porosity and net reservoir rock (part of the gross rock volume that is reservoir) needs to be known. From the model you can also derive the minimum closure depth and spill point as well as the reservoir thickness. The temperature is not taken from the Kyrkheddinge area but from the Ha-1 well in the Lund Geothermal field 10 km away at 770 m depth.

Too calculate the total energy storage capacity in the structure the method suggested by Sopher et al. (2019) was utilized. The equation used was:

$$E = G\theta NV$$

where E equals the total energy storage capacity in MWh, G is the total rock volume inside the structure (gross volume), θ is the porosity where 0 means no pore space and 1 means 100 % pore space, N is net-to-gross reservoir (the proportion of the total rock volume which can be considered reservoir), and V is the energy that can be stored per volume of pore space (kWh/m^3). The gross rock volume (G) can be extracted from the model in ArcScene after the closure point is known. The closure point can be deduced visually from the model with the help of a flat surface which shows when the closure point is reached. The porosity (θ) was estimated for the different levels of the reservoir by Hagconsult AB (1983) and are based on cores and well log interpretations. From those values an average porosity can be calculated for the reservoir. The gross and net thickness for the reservoir was taken from Hagconsult AB (1983) where net thickness was estimated from the porosity values with a cut-off at 23%. The net-to-gross (N) value of the reservoir can be calculated from that. Energy that can be stored per volume of pore space (V) depends on geological factors as well as the CAES plant design. For this thesis a low estimate of 0.1 kWh/m^3 and a high estimate of 1 kWh/m^3 is used. The low value of 0.1 kWh/m^3 is suggested by Allen et al. (1983) and the high value of 1 kWh/m^3 is from the proposed plant in Iowa (Succar & Williams 2008). Flow rate was tested during pump tests in the well Ky-4 and estimated for Sand B (Green Marker).

3.6 Geothermal energy potential evaluation

To evaluate the geothermal energy potential of the Lund Sandstone reservoir in the Kyrkheddinge area the geology was compared with that of the Lund geothermal field. The net sand was calculated for 18 out of 19 wells, data was not available for Vä-1. The top 200 m of the Lund Sandstone was evaluated where possible, not all well logs covered the full extent of the top 200 m (Sk-1: 109 m, Sk-2: 109 m, Ha-1: 119 m, Ha-2: 131 m). The net sand was determined from evaluation of the natural gamma ray logs. The sand units have lower values in the gamma ray logs than the units rich in clay and were separated from the other units by drawing a sand line at around 20 API. All sections below the sand line were regarded as sand. The upper 200 m of the Lund Sandston in the Kyrkheddinge aquifer was then compared with the net sand in the filtered parts (where pumping of water occurs in the wells) of the wells in the geothermal field. The net sand of the geothermal wells was calculated by Aldenius (2017). Here the gamma ray logs were paired with resistivity logs. Sand sections that contain water shows lower values on the resistivity logs. This means that here only porous sand was counted as net sand compared to the new evaluations in this work where all sandy sections were counted.

4 Geothermal energy and various energy storage techniques

4.1 Geothermal energy

Geothermal energy refers to energy from the heat inside earth. The heat is a product of radioactive decay and remnant heat from when earth was formed ~4.5 billion years ago (Glassley 2015). The temperature in the bedrock increases with depth at an average of 30˚C/km but can be more than 100˚C/km in areas with active volcanism and as low as 10˚C in ancient continental crust (Barbier 2002). At high temperatures the geothermal energy can be used to generate electricity and at lower temperatures for heating and industrial processes (Barbier 2002). These low-temperature processes are so-called direct uses and include food processing, drying materials, agricultural activities, aquaculture, paper manufacturing and heating of greenhouses (Glassley 2015). A typical geothermal system for direct use consists of at least two wells where hot water is produced in the production wells and when the heat is extracted the cold water is re-injected into the aquifer through the re-injection wells (Limberger et al. 2018). It is done in a sealed system so the fluids do not react with the oxygen in the air (Erlström et al. 2016). It is also important that the fluids are injected into the same reservoir to keep an even pressure and at an adequate distance from the production wells as not to cool them; in the Lund Geothermal Field it is about 2 km between them (Alm 1999; Erlström et al. 2016).

In Lund the geothermal heat plant has been supplying the district heating system for over 30 years (Aldenius 2017). It uses water from the Lund Sandstone at around 700 m depth (Alm & Bjelm 1995). The temperature is around 20˚C at this depth, however, it has decreased slightly since the start of operations but with modern heat pumps it is still economically feasible to use aquifers with temperatures below this (Alm & Bjelm 1995).

Geothermal plants are usually calculated to last around 30 years (Barbier 2002). This means that the Lund Geothermal plant could be near the end of its operations and it might be time for a replacement. The temperature in the production well had gone down between 2 and 8˚C in 2016 from the start of operations in 1985 (Aldenius 2017). The Lund Sandstone extends to the Kyrkheddinge area at similar depth as in the geothermal field with no major lateral changes in geology (Erlström 1990). This could be of interest to expand on the geothermal energy production to the area south-east of Lund.

According to Barbier (2002) the prerequisites for successful geothermal operations is a good reservoir, the reservoir has to have sufficient permeability in each well for pumping as well as a high temperature and for longevity a large amount of heat store. To not risk corrosion the fluids in the aquifer should have a pH near neutral (Barbier 2002).

There are risks of both air and water pollution in geothermal operations, but with re-injection it is not a major concern (Barbier 2002). With re-injection the risk of land subsidence declines but the risk of induced seismic events increases, although it is suggested that they only increase in number while decreasing in magnitude (Barbier 2002).

As about half of the worlds' energy consumption is for heating, and only a small percentage of the geothermal aquifers available can be used for electricity production, low-temperature uses can make a big dent in the fossil fuel use (Brown & Eisentraut 2014; Glassley 2015). Around 0.15% (0.565 EJ/year) of the world energy supply came from geothermal sources in 2014 (Bertani 2016). About half of that was direct heat use and district heating stood for 13.5% of the total geothermal energy use (Lund & Boyd 2016). The low temperature geothermal energy available in the world for direct use is estimated by to be around 32 EJ/year (Stefansson 2005). This means less than 1% of the geothermal energy available for direct use is utilized (Limberger et al. 2018).

4.2 Energy Storage

To reach their goal for 'clean, secure and affordable energy for all EU citizens' the European Commission wants to diversify the energy sources inside the EU (European Commission 2016). Renewable energy sources are critical in lowering the emission of greenhouse gasses and needs to be integrated in the power grid (Muttaqi et al. 2019). The problem with many renewable sources, like wind and solar power, is that the energy production fluctuates and does not match the electricity demand (Li et al. 2018). To match the energy production from renewable sources with the demand, long- and short-term energy storage is needed (Muttaqi et al. 2019). The following main alternatives to store energy exist today; mechanically (Pumped Hydro and Compressed Air Energy Storage), thermally (Latent Heat and Sensible Energy Storage), Superconducting Magnetic Energy Storage (SMES) and electro chemically (batteries and fuel cells) (Venkataramani et al. 2016).

One of the projects that deals with energy storage is ESTMAP (European Commission 2016) which maps out possible sites for energy storage below and above ground. The underground storage methods suggested in ESTMAP are:

- Compressed Air
- Natural gas
- Hydrogen
- Thermal
- Underground pumped hydro

Compressed Air Energy Storage (CAES) is a relatively new technology and is considered to be one of the most economical and effective methods for large scale and long term storage (Li et al. 2018). The Huntorf CAES Plant in Germany became the first CAES facility in the world when it was finished in 1978 (Succar & Williams 2008). It is a way to store energy during long periods by compressing air and pumping it into a reservoir, when the air is recovered it is used to drive a turbine so the energy can be used for electricity (Succar & Williams 2008). Around 80 % of the electricity production can be regenerated in a CAES plant (Venkataramani et al. 2016). There are three classes of CAES plants described by Venkataramani et al. (2016); Adiabatic, Diabatic and Isothermal. Adiabatic refers to a process where the heat of the compressed air is not lost and is instead used for power generation. In the diabatic process heat is lost to the atmosphere as waste while renewable energy drives the compression and natural gas can be used to reheat the compressed air when needed. An isothermal process allows the air to compress without changes to the temperature. The air can be stored with minimal loss of energy while there is no need for combustion of natural gas for power generation.

A CAES plant consists of five basic components; a reservoir and the machinery which includes a compressor, a turbine, motor or generator and a thermal storage system (Li et al. 2018). It is possible to store compressed air above ground in gas pipes and steel containers but for large scale CAES-operations an underground reservoir is needed as it is both cheaper and more secure (Li et al. 2018).

The storage reservoir requirements are described by Succar & Williams (2008). The needs are similar to those for natural gas storage. The alternatives for reservoirs are; salt domes, hard rock and porous rock. Salt domes are easy to mine, and cavities can be shaped in the way that is needed. Hard rock is expensive to mine while porous rock could be the cheapest way to store air as no mining is needed. Natural gas has been stored in porous rock since 1915 and today 95 % of all natural gas storage is done in porous rock, so at this point the technology for storage is well developed (Li et al. 2018). According to Succar & Williams (2008) a porous aquifer needs to have ade-

quate permeability to work as a reservoir, as well as the porosity, which is what will determine how much air that can be stored. The reservoir should be a closed convex structure, so the air does not escape to the sides. The cap-rock needs to have low permeability to keep the air in and it needs to be able to withstand the increased pressure of the compressed air. The reservoir pressure needs to be high enough to keep tight but not too high for the machinery to work, 39–50 bar was determined to give the best performance. According to Succar & Williams (2008) a problem that can arise, especially if the reservoir is in an abandoned oil or gas field, is that there is residual hydrocarbons. These can react with the oxygen and create compounds that reduce permeability. There is also a risk for increased flammability and combustion in the reservoir.

Right now there are two plants in operation, the Huntorf CAES plant in Germany, which is the smallest one at 310,000 m^3 and the McIntosh plant in the USA, both salt caverns (Succar & Williams 2008; Li et al. 2018). There are two more plants under construction where the largest one, Norton (USA), is a 9,600,000 m^3 hard rock cavern. The other one, The Iowa Energy Park, is in a porous rock formation with only a tenth of the power capacity of Norton, 270 MW compared to 2700 MW (Li et al. 2018). Another three plants using salt rock are planned and two using porous rock formations (Li et al. 2018). A test plant using porous rock was used successfully in Italy until it had to be shut down due to geological disturbances (EPRI-DOE 2003).

Hydrogen can be stored in similar ways as to natural gas, mainly in salt caverns, depleted oil or gas reservoirs, and aquifers (Lord 2009). Hydrogen is a good energy vector with high energy density (Sainz-Garcia et al. 2017). It can be produced by water reduction or electrolysis and stored under high pressure (Shatnawi et al. 2018).. Hydrogen is a small molecule and there is a high risk of leakage, it is also costly, especially in aquifers where it requires a large volume as up to 80 % needs to be cushion gas (Lord 2009).

Thermal energy storage can be done in aquifers as well. By pumping warm or cold water into a water-bearing permeable layer the water in the aquifer will be cooled or heated and the cold or warm water can later be pumped back out when needed (Rudolph et al. 2018). The requirements for thermal energy storage in an aquifer are that the aquifer can handle high flow rates from the wells, the heating and cooling requirements vary with the seasons, and that the thermal loads are preferably above 250 kW (Schmidt et al. 2018). It is preferred that the drift velocity in the layer is low and it should be capped by an impermeable layer so as not to lose the temperature changes to other layers (Rudolph et al. 2018).

Underground pumped hydro utilizes two reservoirs at different levels where one can be above ground (Pickard 2012). It can utilize surplus energy to pump water from the lower reservoir to the upper one, when there is an energy deficit the water can be released from the upper reservoir to the lower one and driving a turbine as it flows down (Pickard 2012). This type of storage requires excavation of a reservoir (Uddin 2012).

5 Geological setting and properties of the Lund Sandstone

5.1 Stratigraphy

The stratigraphical information presented in the following text regarding the Cretaceous deposits is mainly based on the comprehensive work by Erlström (1994). The characteristics of the Lund Sandstone is also largely based on the work by Erlström (1990) and references therein.

The Lund Sandstone is found in the marginal eastern parts of the Danish Basin (fig. 1). This basin is ca 200 km wide and stretches from Poland all the way up to the North Sea. It dates back to the Late Paleozoic; however, it is largely dominated by a Mesozoic fill (fig. 8). The Fennoscandian Border Zone including the Sorgenfrei-Tornquist Zone mark the north-east margin of the basin. The basin was split from the adjacent Vomb Trough and Kristianstad Basin during peak inversion of the Sorgenfrei-Tornquist Zone in the Santonian and Campanian. In south-west Skåne the north-west trending Romeleåsen Fault and Flexure Zone marks the border of the Danish Basin. The uplift, i.e. inversion of previously submerged strata to the north-east of the Romeleåsen Fault Zone, greatly controlled the prerequisites for the formation of the Lund Sandstone in the subsiding margins of the Danish Basin during Santonian–Campanian times.

The Lund Sandstone is one of several units that together make up the ca 1800 m thick Upper Cretaceous–lower Paleogene Höllviken Formation within the marginal parts of the Danish Basin in south-west Skåne (Erlström 1994). The Höllviken Formation consists of, from bottom to top; the Arnager Limestone, Granvik Member, Lund Sandstone, Kyrkheddinge Member, Hansa Member, Kruseberga Member, Limhamn Member, Copenhagen Limestone and Landskrona Member (fig. 9; Sivhed et al. 1999). In comparison to the thick Upper Cretaceous, the Lower Cretaceous is considerably thinner, ca 200m, with a less well defined stratigraphy (Norling 1981).

The 20–60 m thick Cenomanian Arnager Greensand subcrop the Höllviken Formation. It was deposited during a time of widespread marine conditions in northern Europe. In the marginal areas the dominating deposition was glauconitic sands (Larsson et al. 2000).

The lowest member of the Höllviken Formation, and the start of the Upper Cretaceous, is the Arnager Limestone, which is of Turonian and Coniacian age. General subsidence in the area led to even more marine influence and chalk facies spread to the marginal areas which resulted in a dense biomicritic and partly silicified limestone that is up to 75 m thick.

Above the limestone lies the up to 400 m thick Granvik Member, dominated by variably argillaceous limestone. The Granvik Member is followed by a thick Santonian–Campanian succession which is dominated by mixed clastic deposits, i.e. the Lund Sandstone. This unit increases significantly in thickness towards the bounding Romeleåsen Fault, as a result of subsidence and high rates of sedimentation coupled to erosion of the uplifted area north-east of the Romeleåsen Fault Zone. As the rate of subsidence was consistent with the amount of sediment entering the basin margin

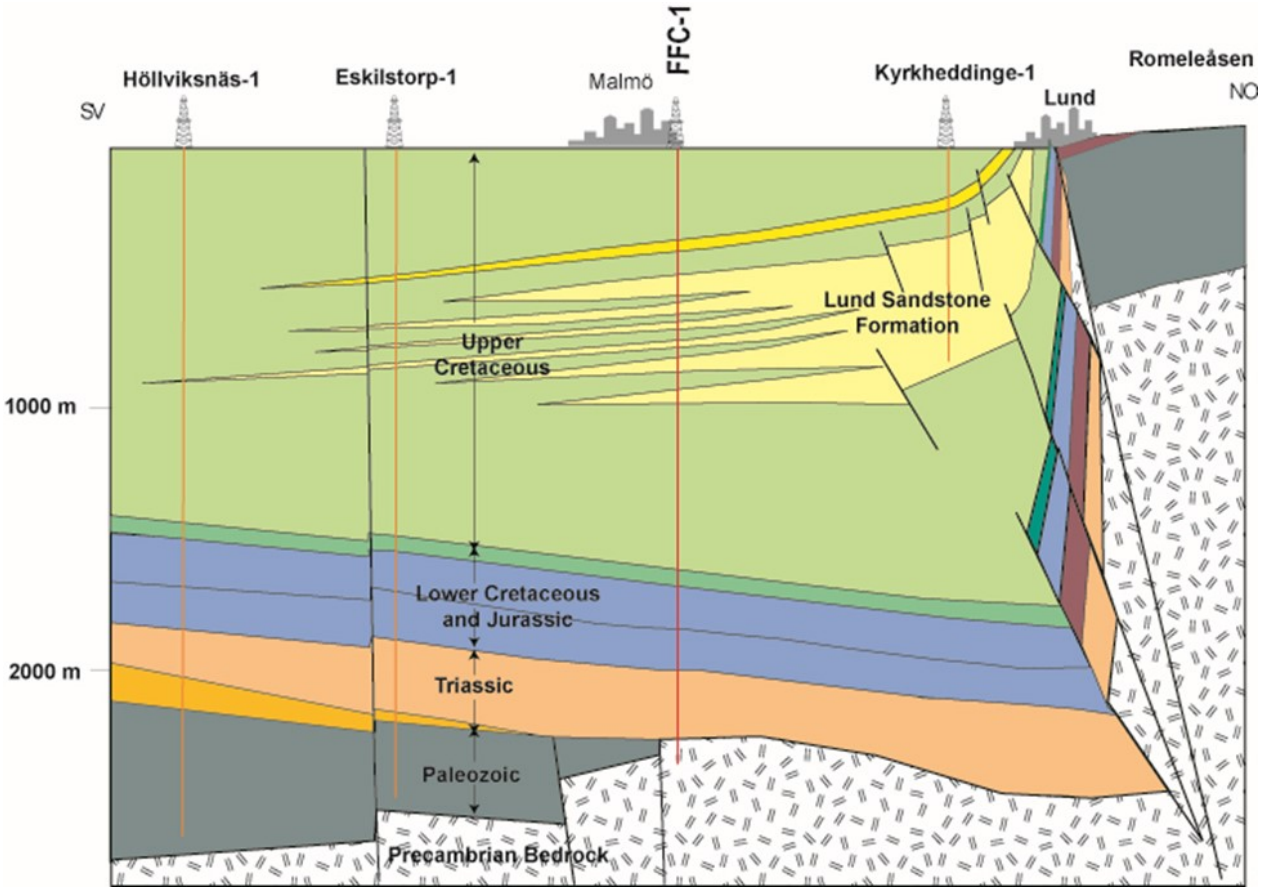

Fig. 8. Cross-section showing the stratigraphy from the Romeleåsen Horst in the north-east to Höllviken in the south-west. It shows the Lund Sandstone getting deeper to the south-west and then thinning out (modified from Erlström 2017).

there was enough accumulation space to keep the depositional setting relative constant and consequently resulting in thick sedimentary successions dominated by proximal deltaic sandstone beds. Further out in the Danish Basin the Lund Sandstone is considerably thinner and dominated by fine-grained distal sandstone and siltstone. Synchronous Campanian deposits are also found in the Vomb Trough and in the Kristianstad Basin (Erlström 1994). Similar thickening Campanian strata towards the Christiansö Fault are in addition found in the Hanö Bay Basin (M. Erlström, Lund, pers. Commun., 2019).

The Lund Sandstone is sub-cropping the Maastrichtian, which is divided into three different members, with the lowest one being the Kyrkheddinge Member. During the Maastrichtian the subsidence continued in the Danish Basin and in places this sedimentary succession is up to 700 m thick. This is related to the fact that the Maastrichtian was characterized by an overall rising sea-level and Maastrichtian deposits covered previously most of Skåne and south Småland (Lidmar-Bergström 1982). The Kyrkheddinge Member is dominated by fine-grained carbonate-rich sediments (Sivhed et al. 1999). At the top of the Maastrichtian strata is the Kruseberg Member which is a chalky formation with chert layers at the top. In between these two layers is the Hansa Member which as the Lund Sandstone is dominated by sandstone beds. Clastic sediments coming from Romeleåsen Horst formed a 50-meter-thick succession dominated by poorly consolidated, medium- to coarse-grained sandstone beds. Some beds are also conglomeratic. The Hansa Member indicates that rejuvenated uplift occurred in the middle Maastrichtian, involving the Romeleåsen Horst, which resulted in coarse clastic deposits in the Lund area (Sivhed et al. 1999).

The Kruseberg Member marks the uppermost part of the Cretaceous and at the top of the Höllviken Formation lies three Paleogene members (fig. 9); the Limhamn Member and the Landskrona Member are Bryozoan limestones whereas the Copenhagen Limestone is a bioturbated, fine-grained limestone with chert layers. Above the Höllviken Formation is the Lellinge Greensand, which is found as scattered occurrences south of the city ofMalmö and in the Svedala area (Sivhed et al. 1999).

5.2 Petrological and physical properties

Based on cores from the Kyrkheddinge area south-east of Lund, Erlström (1990) found that the Lund Sandstone is dominated by four lithofacies with distinguishing petrological and physical properties. The four facies are; quartzose sandstone, calcareous sandstone, arenaceous limestone and argillaceous limestone. The sandstone mostly exhibits high porosity and permeability but also contain well-cemented parts that are less permeable.

5.2.1 Quartzose sandstone facies

The quartzose sandstone facies is the facies with both the highest and lowest porosity and permeability, de-

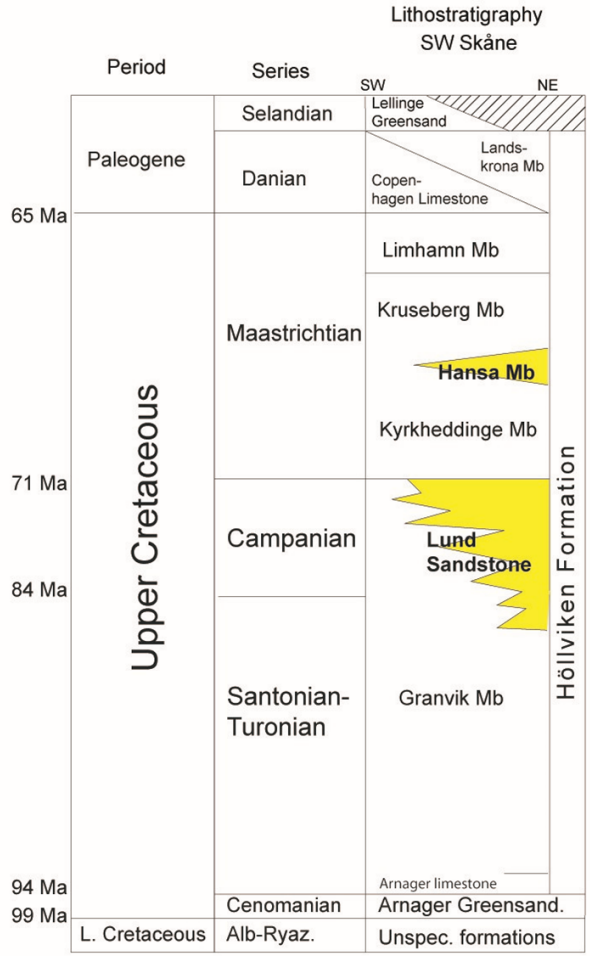

Fig. 9. Lithostratigraphy of the Upper Cretaceous in south-western Skåne. The Lund Sandstone is part of the Höllviken Formation. It is at the top of the Granvik Member, thinning out from the north-east towards the south-west (modified from Sivhed et al. 1999)

pending on if it is cemented or not. The usually thin beds, often <1 m, consists of mainly medium- and coarse-grained polycrystalline quartz which can be cemented with silica or sparite. The porosity can reach up to 38% and the non-cemented beds generally have a porosity >25%. The cemented beds have generally a porosity that is <10%. However, porosities <5% are also noted. The variably well-cemented quartzose sandstone beds have commonly a permeability $<10^{-3}$ mD while the non-cemented beds can have much higher permeabilities of $>10^{4}$ mD.

5.2.2 Calcareous sandstone facies

The calcareous sandstone facies often display porosities between 20 and 30% and permeabilities of 10–300 mD. However, this facies is commonly cemented with sparite, which at times leads to voids and pores being more or less completely filled with cement. The corresponding porosities are hence, generally <10%. The calcareous sandstone is less well sorted and more heterogenous in comparison with the quartzose sandstone. The beds display mixed grain-sizes from fine- to coarse-grained and there is commonly a significant skeletal component of up to 14% (Erlström 1990). The calcareous content comes from three components; biomicrite, sparite and skeletal debris, and comprise around 30 to 60% of the bulk. The quartz component is around 60%. The poorly sorted texture is interpreted to be caused by intense bioturbation.

5.2.3 Arenaceous limestone facies

The sandstone facies is often interbedded or alternating with the two limestone facies. The arenaceous limestone consists of a tight heterogeneous fabric of biomicrite and a non-micritic matrix of clays, organic material, fossils and detrital grains of mainly fine- to coarse grained quartz. The arenaceous limestone has relatively high porosities of 10–20%. Parts of this porosity is related to the content of smectitic clays. The clay content also causes the low permeabilities that are generally <0.1 mD.

5.2.4 Argillaceous limestone facies

The argillaceous limestone is sometimes hard to distinguish from the arenaceous limestone and usually occur in connection with the latter limestone beds. It has similar porosity as the arenaceous limestone, i.e. 10–20% but usually slightly lower permeabilities of 0.1–10^{-4} mD. It has a patchy texture of fine and very fine-grained detrital quartz and some feldspars and an argillaceous biomicritic matrix. It has a lower quartz content than that of the arenaceous limestone.

5.3 Depositional environment

During the late Campanian the European Cretaceous shelf seas may have reached its largest extent (Tyson & Funnell 1987). Basin type facies was spread across most areas that were not tectonically active (Tyson & Funnell 1987). General subsidence coupled with inversion and down warping of underlaying sediments during the Late Cretaceous led to complex geology in the area (Pegrum 1984). Along the Romeleåsen Horst clastic deposition started during the Late Santonian and led to thick clastic deposits along the horst thinning out to the south-west (Erlström 1990). The sediments were mainly accumulated in three different depositional centra; the Kyrkheddinge, Lund and Landskrona areas with possibilities for more undiscovered centras along the south-west side of the Romeleåsen Horst (Erlström 1990).

Erlström (1990) described the deposits as clastic dominated shore-line type. According to Heward (1981) these kind of deposits have four main geometries and origins; transgressive sheet sands of deltaic association, transgressive sheet sands of non-deltaic association, regressive sheet sands and linear sand bodies. The Lund Sandstone is dominated by transgressive sheet sands and regressive sheet sands associated with a prograding delta (Erlström 1990). Transgressive sheet sands in deltas are the result of delta lobe abandonment or submergence during rapid rise of the sea level and the regressive sheet sands are generated due to the high sedimentation rate in an expanding source area in the prograding delta (Heward 1981).

The four main facies in the Lund Sandstone were interpreted by Erlström (1990) to be accumulated in different types of environment. The quartzose sandstone beds are interpreted to be longshore sandbars and beach sand, the calcareous sandstone is thought to

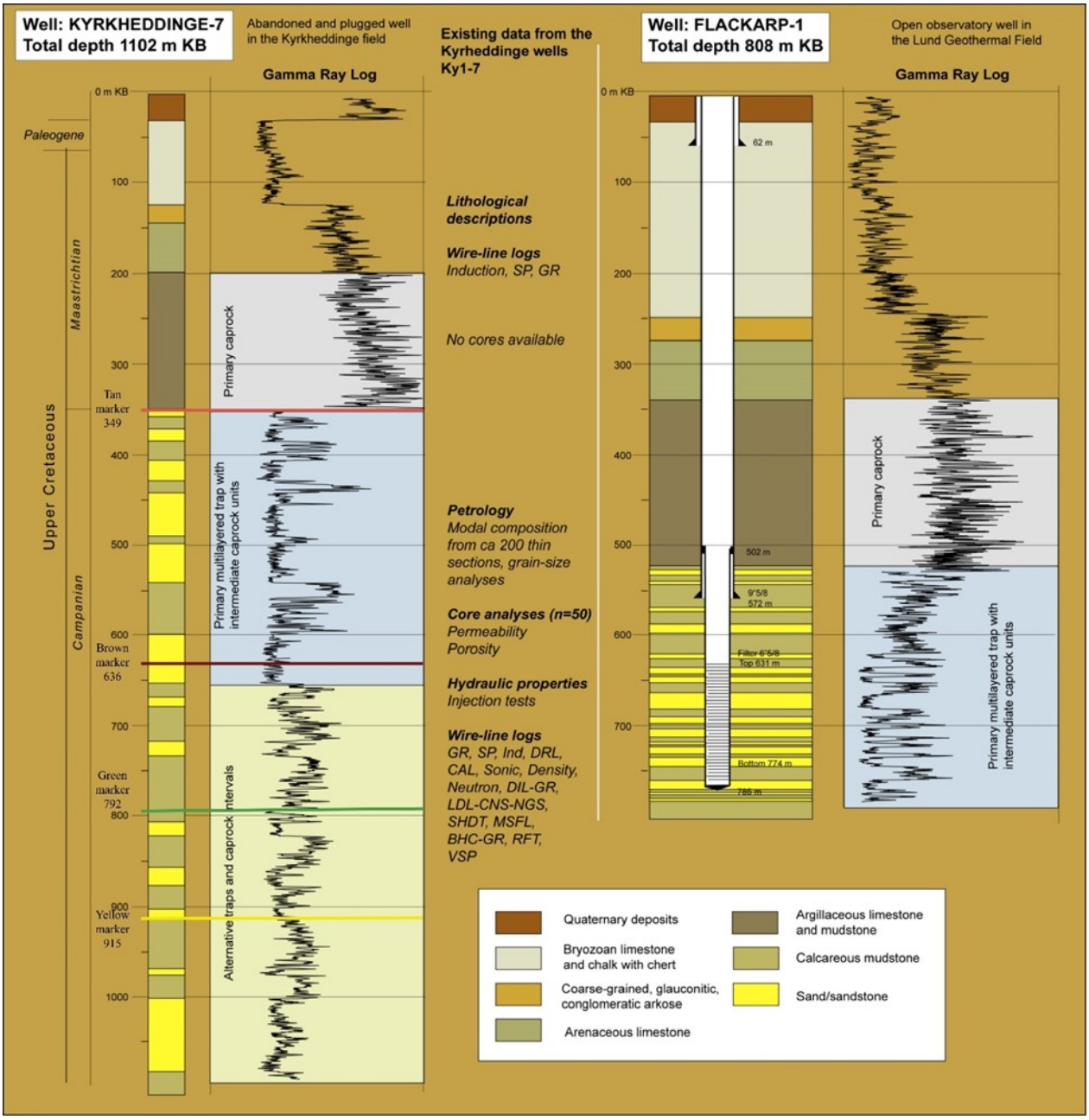

Fig. 10. Illustration of two type sections of the subsurface geology in the Lund-Kyrkheddinge area exemplified by the Ky-7 and Fl-1 wells. The top (Tan Marker) and base (Yellow Marker) of the Lund Sandstone is shown in the well Kye-7 as well as the Green and Brown markers (modified from Bjelm et al. 2014)

be channel distributary mouth bars, arenaceous limestone derives from offshore delta front or proximal delta, and argillaceous limestone are thought to have accumulated in interdistributary bays and the distal delta.

5.4 Distribution, thickness and depth

The distribution, thickness and depth of the Lund Sandstone is described by Erlström (1990) and much of the information is taken from there. The Lund Sandstone is distributed parallel to the Romeleåsen Horst from Skurup in the south-east to north of Landskrona in the north-west (fig. 11). It is also recorded in boreholes in the Öresund area between Helsingborg and Helsingör (Larsen et al. 1968). It is thickest and has its shallowest position close to the Romeleåsen Fault and Flexure Zone thinning out and getting deeper further out in The Danish Basin to the south-west. Outside of the flexure zone the top of the sandstone dips gently towards the south-west. The deepest position of the Lund Sandstone is around 650 ms TWT (two-way travel time) and the shallowest is around 150 ms TWT north-west of Lund. In the two wells in the studied area where the boreholes have penetrated the Lund Sandstone it is 310 and 565 m thick (in Mo-1 and Ky-7 respectively). According to Erlström (1990) the sandstone is up to 845 m at its maximum thickness and the top of the Lund Sandstone can be traced to between 8 and 15 km south-west of the Romeleåsen Horst. The sandstone extends at least 100 km from

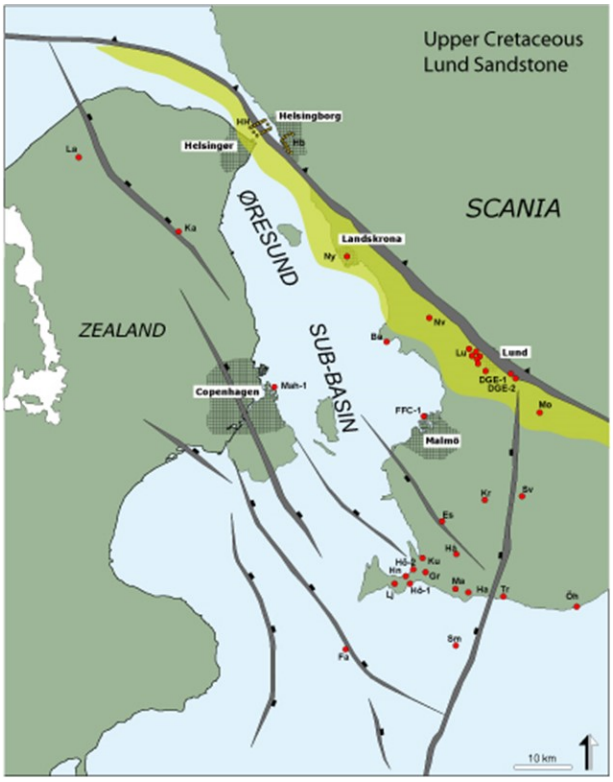

Fig.11. Map over western Skåne and eastern Denmark with the distribution of the Lund Sandstone in yellow. It is bordered by the Romeleåsen fault and flexure-zone to the north-east (modified from Erlström). Red filled circles refer to deep wells (see Sivhed et al. 1999; Lindström et al. 2018).

south-east to north-west (Bjelm & Lindeberg 1994).

In the Lund-Kyrkheddinge area poorly consolidated medium-grained sandstones dominate the succession. The upper c. 200 m of the Lund Sandstone in the Kyrkheddinge area is dominated by the two sandstone facies described above. The total thickness as well as the number of sandstone beds in the Lund Sandstone decreases significantly to the south-west, i.e. distally out into the Danish Basin. The Lund Sandstone is increasingly heterogenous towards the Romeleåsen Fault and Flexure Zone with a slight fining of the deposits towards the north-west and south-east. The dense interbeds are difficult to correlate due to limited lateral extent of cementation and their lateral extent is often less than that of the distance between the boreholes.

5.5 Physical, hydraulic and chemical properties

5.5.1 Porosity and permeability

The porosity and permeability of the Lund Sandstone is described by Erlström (1990). Analytical results from the different facies porosities and permeabilities are illustrated in fig. 12. The porosity and permeability differ due to different grain size, sorting and cementation. According to Erlström (1990) the quartzose sandstone facies has the highest porosity and permeability, when uncemented, reaching >40% and $>10^4$ mD respectively. Cemented beds of quartzose sandstone display the lowest values for both porosity and permeability. The porosity values are generally <10% and sometimes <5% and the permeability values between

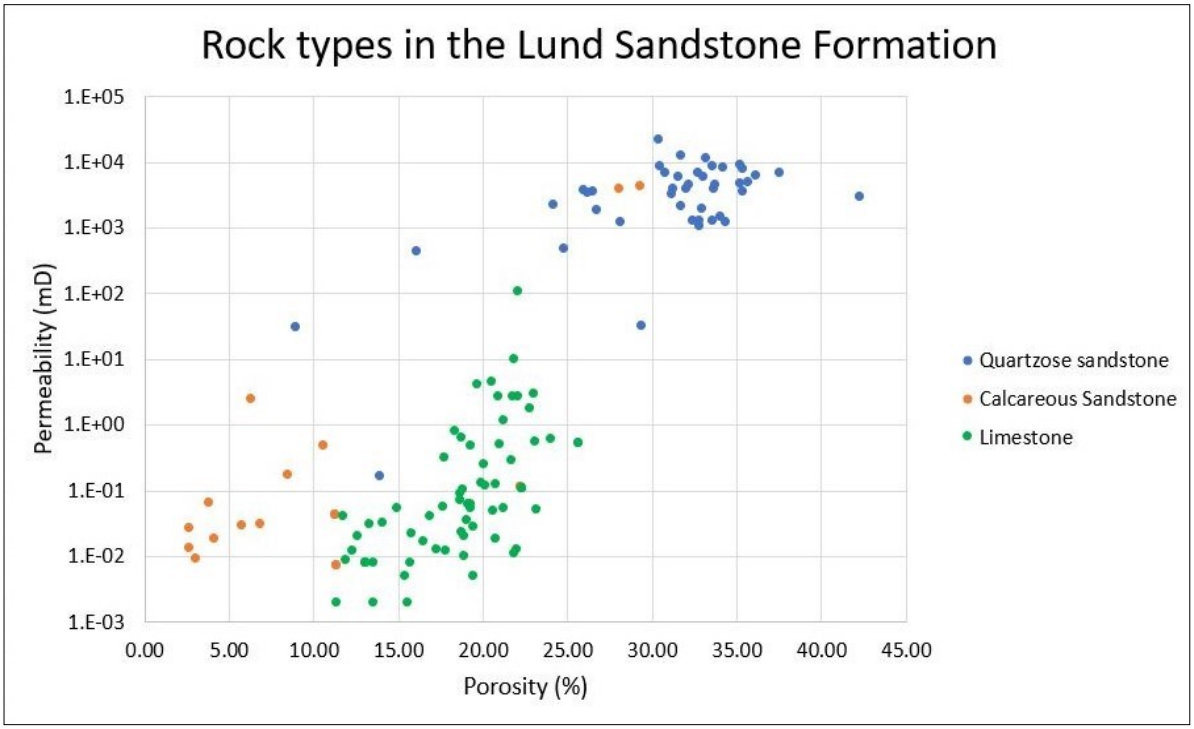

Fig. 12. Diagram showing permeability and porosity of the different facies in the Lund Sandstone. The quartzose sandstone is the facies with the highest porosity and permeability, but porosity can be <10 % and permeability can be <1 mD. The calcareous sandstone has the lowest porosity and permeability and is generally <15 % porosity and <1 mD in permeability. The two limestone facies are hard to differentiate but they fall in the middle when it comes to porosity and vary in

Table 3. The chemical composition of the fluids in the wells Fl-1 and Vä-1 in the Lund Geothermal field. Also includes the pH, redox potential and conductivity. These could be indicative of the conditions in the Kyrkheddinge area.

Parameter /well	*Fl-1*	*Vä-1*
pH	6.5	6.5
Redox potential (mV)	-52	-26
Conductivity (ms/cm)	83	72
Chloride (mg/l)	38 000	35 800
Sulphate (mg/l)	20	1.0
COD (mg/l)	1220	2030
Ammonium (mg/l)	27.8	20.5
Nitrate (mg/l)	<0.002	<0.002
Nickel (mg/l)	<0.005	<0.008
Iron (mg/l)	38.4	53.0
Potassium (mg/l)	87	88
Silicon (mg/l)	6.2	6.1
Aluminum (mg/l)	0.40	0.32
Strontium (mg/l)	1350	1050
Calcium (mg/l)	7200	6500
Sodium (mg/l)	13 100	13 400
Copper (mg/l)	0.07	0.10
Manganese (mg/l)	0.23	0.24
Lead (mg/l)	1.00	0.04
Silver (mg/l)	0.11	0.09
Magnesium (mg/l)	1130	980
Phosphate (mg/l)		0
Bicarbonate (mg/l)		104
Total salinity (%)	6.2	5.8

10^{-3} and 10^{-4} mD. The calcareous sandstone beds display somewhat lower values with porosities between 20 and 30% and permeabilities ranging between 10 and 300 mD in the uncemented parts, whereas where the beds are cemented with sparite the porosity decreases to 10% and the permeability to as low as 10^{-2} mD. The two limestone facies have similar porosities of around 10 to 20% but the argillaceous limestone has lower permeability of $0.1–10^{-4}$ mD while the arenaceous limestone is around 0.1 mD.

5.5.2 Temperature and pressure

Data from the start of production in the Lund Geothermal field 1985 and tests by the department of engineering geology of Engineering LTH at Lunds Tekniska Högskola (1984) both show temperatures of around 20–21˚C at an aquifer depth mid-point of around 700 m. The tests show that the formation pressure is slightly higher than hydrostatic pressure (Hagconsult AB 1983).

Table 4. The gas composition in the wells Fl-1 and Vä-1 in the Lund Geothermal Field. It comprises of mainly Nitrogen (>90%) and has a methane content of less than 5%. These could indicate how the conditions are in the Kyrkheddinge area.

Gas	*Fl-1*	*Vä-1*
Nitrogen N2	90%	92.5%
Methane CH4	3.0%	1.9%
Carbon dioxide CO2	0.9%	1.0%
Argon Ar +(O2)	2.8%	2.0%
Helium He	0.4%	0.4%
Hydrogen H2	traces	0
Hydrogen sulfide H2S	<1 ppm	<1 ppm
Carbon monoxide	<1 ppm	<1 ppm
Ammonia NH3	<0,5 %	<0,5%

Table 5. Estimated formation fluid composition in the well Ky4 in the Kyrkheddinge area.

Water Composition	*Ky-4 (%)*
Sodium chloride	3.50
Potassium Chloride	0.59
Calcium chloride	2.10
Magnesium chloride	0.25

5.5.3 Chemical composition of formation fluids and gases

The formation fluid composition was analyzed in the Lund Geothermal Field before operations started in the wells Fl-1 and Vä-1 (Lunds Tekniska Högskola 1984). The data comes from analyses performed during 40 days of pumping tests. All analyses were performed by the laboratory at the Division of Engineering Geology, LTH at Lund University. Both the chemical composition and the gas content of the geothermal water was tested and showed similar results for both wells. Chemical composition of the formation fluid is shown in table 3 and gas content in table 4. An average chemical composition of the formation fluids from the Ky-4 well in the Kyrkheddinge area was also analyzed by the water laboratory of SGAB, Uppsala (table 5).

6 Results

6.1 Digital model

The work resulted in a 3D model in ArcScene which display subsurface structure of the Lund Sandstone. Both the top and base is modeled as well as the key horizons (Green Marker and Brown Marker) (fig. 13). The model successfully shows the structural outline of the Lund Sandstone. Moreover, the model gives the necessary input to estimate the depths, areas and closed volumes of the structures.

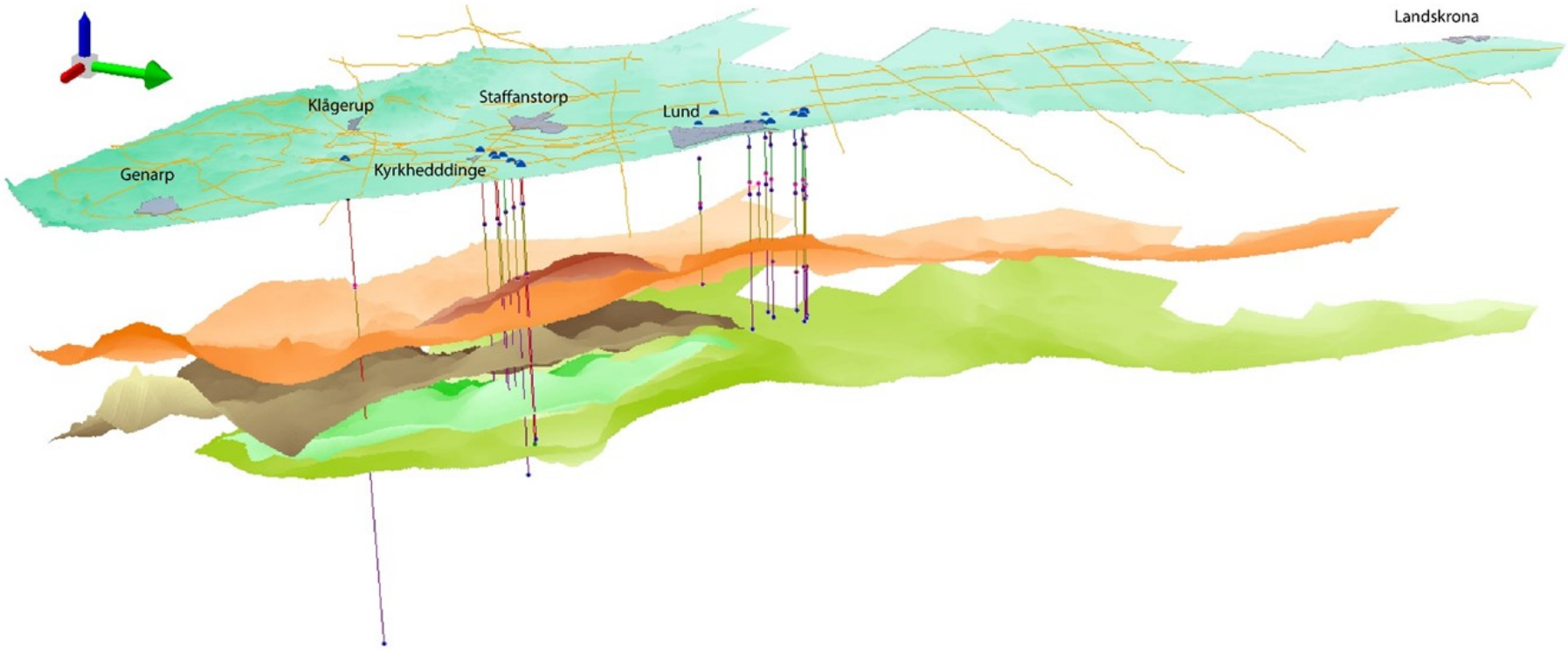

Fig. 13. 3D model showing all the marker beds mapped in the Lund Sandstone. At the top is ground level with seismic lines in yellow and wells as blue dots and lines going down to their actual depth. In the Kyrkheddinge area the Tan Marker is the top layer, which is also the top of the Lund Sandstone. The Tan Marker has not been possible to map outside the Kyrkheddinge area, partly because the lack of corresponding dense seismic grid. The Orange Marker is actually slightly deeper than the Tan, but it is the closest layer to the top of the Lund Sandstone that is mapped out in the rest of the area. Furthest down in a mossy green is the Yellow Marker which is the base of the Lund Sandstone (not yellow in model due to not being available as a choice in the program). In between the top and base is the Brown and Green Marker which are two important stratigraphic boundaries inside the Lund Sandstone, which have possible properties for energy storage. The view is from the Romeleåsen Horst towards west. The green arrow points to the north.

6.2 Suitability for Compressed Air Energy Storage

Two closed structures were identified in the Kyrkheddinge area in the model. One below the Green Marker (top at 716 m) (fig. 14) and one below the shallower Brown Marker (top at 568 m) (fig. 15). Whereas the Green structure is a single large dome structure, the Brown structure is smaller and interpreted as two individual, partly interconnected dome structures (fig. 16).
The key properties for compressed air storage are presented in table 6. For the Green structure the permeability and porosity are excellent. Both properties are clearly above the necessary values for being classified as an excellent reservoir. To be considered an excellent reservoir permeability needs to be >500 mD and porosity >16%. A low estimate for porosity in the Green structure is 23% which would still be above the excellent range. Presently, there is no energy storage plant planned in the area, so the Total Reservoir Volume (the volume of pore space above the spill point compared to the size needed for CAES operation) is difficult to assess but the volume is about 3.6 times as large as the largest CAES operation in construction; the Norton plant in the USA. This would give the structure a score of 3 (see table 2) which is satisfactory since it is more than 3 times as large as necessary. The total closure rating of 0.43 is too low and would disqualify the structure since more than half of the reservoir ought to be above the spill point. This is based on the reservoir having the same thickness outside of the structure as in the structure. Well data also shows that it might not be closed to the north-east. The depth to the top of the reservoir is 716 m which gives a satisfactory score of 3, to be considered good the top of the structure should be located above 670 meters depth. The pressure in the reservoir is 77.5 bar which is to high according to the ranking criteria (score=1), based on the pressure capacity of 14–69 bars with the turbomachinery in the 1982 EPRI study (Succar & Williams 2008).With newer machinery this pressure might not be considered unsatisfactory. The Lund Sandstone was deposited as a delta and the channel sandstones are considered a good type of reservoir.

Residual hydrocarbon is not tested in the wells in Kyrkheddinge, but the well Fl-1 in the Lund Geothermal field show a methane content of 3% and Vä-1 in the same area has a methane content of 1.9%. This is considered satisfactory but to be an excellent reservoir the residual hydrocarbon content should be below 1%.

Regarding the caprock for the Green structure there is no data available on cap rock leakage or cap rock threshold pressure. The cap rock permeability is 0.062 mD which is considered satisfactory, to be good it would need to be $<10^{-5}$ mD. The thickness of the cap rock is between 6–26 m, which is good as anything above six meters is considered a good thickness.

The Brown structure is not studied in the same detail as the Green and because of this there are some

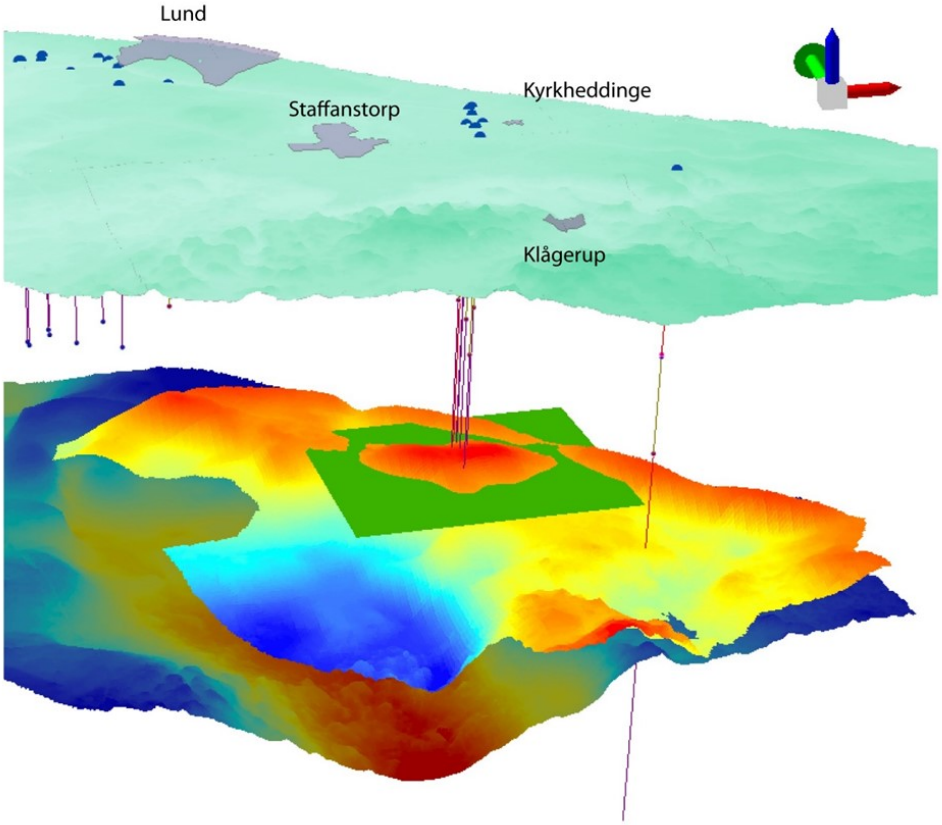

Fig.14. 3D model showing the dome structure in the Green Marker. The green plane is horizontal at 770 meters below sea level and shows the level the green structure is closed at. Green arrow pointing north. Map is showing ground level, Green Marker and Yellow Marker. Blue dots are the wells used in the study with lines showing their depth.

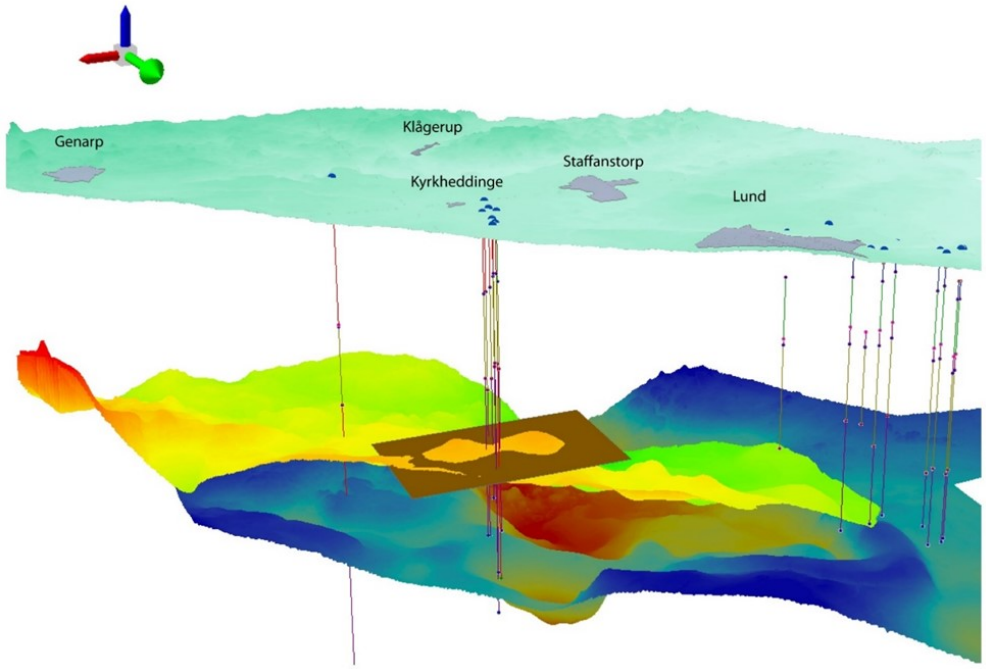

Fig. 15. 3D model showing the Brown structure as one closed structure with two peaks. Horizontal plane at 595 meters below sea level. Ground level, Brown Marker and Yellow Marker shown. Blue dots are the wells used in the study with lines showing their depth. Green arrow is pointing north.

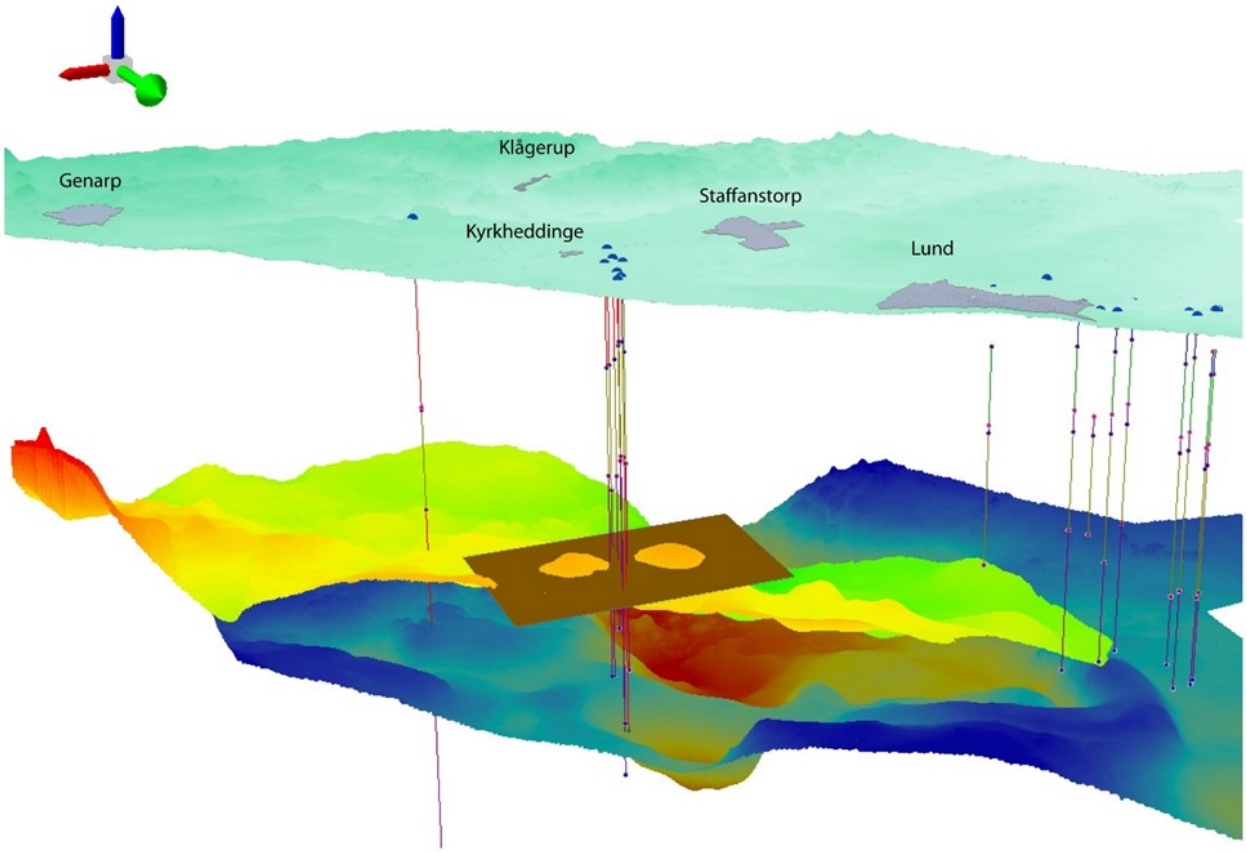

Fig. 16. 3D model showing brown structure as two separate dome structures. Horizontal plane at 590 meters below sea level. Ground level, Brown Marker and Yellow Marker shown. Blue dots are the wells used in the study with lines showing their depth. Green is arrow pointing north.

Table 6. CAES ranking criteria from Succar & Williams (2008) with the data for the structure found in the Green Marker as well as data for the Brown Marker. For the Brown Marker the size and closure rating are calculated for both the domes as one structure and as separate structures. Data is based on the 3d model as well as the reports from the Natural Gas investigations.

Structure	*Green structure*	*Score*	*Brown structure*	*Score*
Permeability (mD)	1700	5		
Porosity (%)	28.5	5	32	5
Total Reservoir Volume (V_R/V_S)	3.6	3	0.17–0.88	4
Total Closure Rating (h/H)	0.43	1	0.20–0.34	1
Depth to Top of Reservoir (m)	716	3	568	4
Reservoir Pressure (bar)	77.5	1		
Type of Reservoir	Channel Sandstone	4	Channel Sandstone	4
Residual Hydrocarbons (%)	1.9–3	3	1.9–3	3
Cap rock leakage	No data	2	No data	2
Cap rock Permeability	0.062	3		
Cap rock Threshold Pressure (bar)				
Cap rock Thickness	6-26	4	2	3
CAES score using ranking table from Succar and Williams (2008)		34/60		26/60
Available		55		37
Score percent (%)		64		70

data missing and some of it is not as certain. There are no data available for permeability and the porosity is uncertain due to extreme washouts during testing (i.e. poor hole conditions) but is estimated at 32% by Hagconsult AB (1983). The Brown structure can be divided into two smaller dome structures. If both could be utilized as a reservoir the total reservoir volume is good. It is 0.9 which means it is slightly smaller than the aforementioned Norton plant. If the Brown structure is used as two separate dome structures, they would both be unsatisfactory at 0.2 and 0.3 when compared to the Norton plant, but they are both larger than the small scale Huntorf plant in Germany. The 568 m depth to the top of the formation is good, which is not far off from an excellent score of 430–550 m. It is the same type of reservoir as the Green structure, channel sandstones, and the residual hydrocarbon can be assumed to be similar, i.e. 1.9–3%. The cap rock is estimated to be only two meters thick which is satisfactory, but it needs to be above 6 m to be classified as good.

Other important reservoir properties are shown in table 7. The areas of the different structures are according to the model calculations $7*10^6$ m^2 for the Green Structure and $3.1*10^6$ m^2 for the Brown structure when both dome structures are connected. For the separate Brown structures, the areas are $1.1*10^6$ m^2 for the North structure and $1.0*10^6$ m^2 for the South structure. According to model calculations the gross volumes for the structures are $1.7*10^8$ m^3 for the Green structure, $3.0*10^7$ m^3 for the Brown structure, $1.10*10^7$ for the North structure and $5.9*10^6$ for the South structure. Pore volume with 28.5 % porosity for the Green structure and 32 % for the Brown structure gives, and net sands of 0.7 for the Green structure and 0.9 for the Brown (Hagconsult AB 1983) gives pore volumes of; $3.48*10^7$ m^3 for the Green structure, $8.47*10^6$ m^3 for the Brown structure, $3.12*10^6$ m^3 for the North structure and $1.66*10^6$ m^3 for the South structure. The model shows a minimum closure depth of 716 m and a closure spill point of 770 m for the Green structure. The Brown structure has a closure depth of 568 m and a spill point of 595. For the North structure the depths are 568 m and 590 m, respectively and for the South structure they are 571 m and 590 m.
The temperature was measured in the Lund geothermal field before the geothermal operations started. It showed 22 ˚C at a depth of 609–709 m in the well Ha-1 which is the closest depth to the Green structure. The well Sk-2 had a temperature of 20.8 ˚C at a depth of 262–669 m which is the closest to the Brown structure. Data on reservoir pressure is only available for the Green structure and it shows a formation pressure of 77.5 bar. The Green structure scored 38 out of 60 in the ranking based on the Succar & Williams (2008) assessment model and the Brown structures scored 26 out of 60. The lower score is partly caused by the fact that there are several property values missing in the data base.

The energy storage capacity is estimated to be between 3,480 GWh and 34,800 GWh for the Green structure. If the same values for porosity and net reser-

Table 7. Additional calculated properties for CAES operation (Succar & Williams 2008; Sopher et al. 2019). The Brown Structure is both described as one closed structure and as two separate structures, one structure to the north and one to the south. Data is based on the 3d model as well as the reports from the Natural Gas investigations.

Closure	*Green*	*Brown*	*Brown N*	*Brown S*
Area of closure (m2)	6.97E+06	3.14E+06	1.10E+06	1.02E+06
Gross rock volume (m3)	1.69E+08	3.00E+07	1.11E+07	5.89E+06
Pore volume (m3)	3.48E+07	8.47E+06	3.12E+06	1.66E+06
min closure depth (mBSL)	716	568	568	571
closure spill point (mBSL)	770	595	590	590
Reservoir max thickness (m)	54	27		
Confidence in structure	Low	Moderate	Moderate	Moderate
reservoir temperature (˚C)	22	20	20	20
reservoir pressure (bar)	77.5			
CAES score using ranking table from Succar and Williams (2008)	38	26		
Energy storage Capacity Low Estimate (MWh)	3,479,809	846,684	312,327	165,608
Energy storage Capacity High Estimate (MWh)	34,798,093	8,466,840	3,123,273	1,656,088
Flow rate (m^3/h)	40,000			

voir rock volume are applied to the Brown structures the energy storage capacities are between 620 and 6200 GWh for the Brown structure, 230–2300 GWh for the North structure and 120–1200 for the South structure.

Hagconsult AB (1983) estimated the gas flow rate for Sand B (Green Marker) to be 40 000 m^3/h, which is around 13 kg/s, in well Ky-4. There are no corresponding data available for the Brown structure.

6.3 Geothermal energy potential of the Lund Sandstone

The top 200 m of the Lund Sandstone in the wells were compared. For some of the wells in the Lund Geothermal Field data was not available for all of the 200 m (Sk-1, Sk-2, Ha-1, Ha-2 and Vä-2) and no data was available for Vä-1. The net sand was generally lower in the Kyrkheddinge area with wells having net sand as low as 34% (Ky-1). The Kyrkheddinge area has three wells with 70% net sand or above (Ky-2, Ky-4 and Ky-7) and a fourth one above 50% (Ky-6). In the geothermal field all four of the production wells (Sk-1, Sk-2, Ha-1 and Ha-2) are above 70% and all the injection wells (Vä-2 – Vä-6) are above 50% net sand (table 8). The net sand was calculated for the filtered parts of the geothermal wells (Aldenius 2017). Here the net sand was determined with resistivity logs as well as natural gamma to see if they contained saline formation water (table 9). The net sand varies between 69 and 83% for the production wells and 50–58% for the injection wells. This corresponds to 43–72 m sand for the production wells and 63–78 m sand for the injection wells.

7 Discussion

One of the goals of this study was to test if using ArcGIS and ArcScene is a good way of digitalizing and visualizing older analog data. The result is a 3D model of the sandstones where each marker bed can be visualized with detailed undulations. The model is useful for visualizing, identifying and making volumetric calculations of structures, such as the dome structures examined in this study. Even though the model facilitates the analysis of the structures it is still affected by the same problems and difficulties that the analog data have. The main problem is the heterogeneities in the geology and therefore the difference in velocities. This makes calculations from TWT to meters difficult and the results are not very accurate. The model is only visualized as layers because when trying to create a block model there is no smoothening and there are not enough details, this also makes it difficult to create cross-sections from the model. A method to

Table 8. Table showing net sand of the top 200 m of the Lund Sandstone in the Kyrkheddinge area as well as the Lund Geothermal Field and the well Mo-1 which is south of the Kyrkheddinge area and Fl-1 which is by the Geothermal field. The net sand was calculated with natural gamma logs and resistivity logs. The result is shown both as a percentage and in total meters. All 200 meters could not be evaluated for Sk-1, Sk-2, Ha-1, Ha-2 and Vä-2 due to available logs. Vä-1 could not be evaluated at all.

Kyrkheddinge area	*Net sand (m)*	*Net sand (%)*	*Total measured*	*Depth to top (m)*
Ky-1	68	34	200	422
Ky-2	145	72.5	200	338
Ky-3	77	38.5	200	490
Ky-4	140	70	200	399
Ky-5	93	46.5	200	432
Ky-6	132	66	200	369
Ky-7	150	75	200	347
Lund Geothermal Field				
Sk-1	138	72.6	190	510
Sk-2	93	85.3	109	534
Ha-1	88	73.9	119	538
Ha-2	97	74.0	131	529
Vä-2	95	51.6	184	464
Vä-3	101	50.5	200	412
Vä-4	130	65.0	200	420
Vä-5	133	66.5	200	416
Vä-6	114	57.0	200	422
Others				
Mo-1	82	41.0	200	616
Fl-1	97.5	48.8	200	519

Table 9. Gross and net sand in the wells used at the geothermal plant in Lund. The production wells have around 70 % sand while the injection wells are closer to 50 %. The net sand in meter is more similar at about 60-80 m except the production well Sk1 at only 43 m.

Production well	*Gross Sand (m)*	*Net sand (m)*	*Net sand (%)*
Ha-1	100	70	70
Ha-2	90	62	69
Sk-1	61	43	70
Sk-2	87	72	83
Injection well			
Vä-2	135	74	55
Vä-3	125.5	63	50
Vä-4	147	78	53
Va-5	120	69	58

visualize faults in the model would make it more sufficient for energy storage investigations as faults can have a large effect on the storage abilities of a structure. To get the full use out of the data another program might have been useful to incorporate more well data and seismic profiles and to create cross-sections, but for finding structures and calculating their size ArcScene is satisfactory. The digitalization of the isochron maps is time consuming and for large scale work another method than tracing the lines is recommended. There are ways to automate the tracing, but the maps need to be cleared from other data before or after as the computer cannot distinguish between isochron lines and other information on the maps.

When it comes to the possibilities for CAES in the Kyrkheddinge area two closed anticlinal structures could be found in the model. One beneath the Green Marker and one below in the shallower positioned Brown Marker. The Green Structure is the largest of the two with a pore volume that could be more than three times as large as the largest CAES plant in planning. The size is mainly an economic issue. It has excellent values for permeability, porosity and cap rock thickness and the channel sandstones of the Lund Sandstone are good reservoirs (fig. 17). The cap rock permeability is a bit too high but still satisfactory and the reservoir is a bit too deep which makes drilling and well construction more expensive (fig. 18). There is a risk of high amounts of hydrocarbons, but this is only measured in other parts of the Lund Sandstone, where the values are still satisfactory, so the actual values for the structure is not known. The biggest problems with the structure are the closure rating and pressure. The pressure of 77.5 bar is deemed too high by Succar & Williams (2008), which is based on an 1982 EPRI study. The max pressure that is deemed usable is based on what the machinery can handle so with more modern machinery higher pressures might be possible for successful CAES operations. The closing rating is based on average thickness of the reservoir and not exact measurements. This means that if the reservoir is thinner than the average at the edges of the structure the closure rating could be more suited for operations. In addition to better knowledge on the closure rating and hydrocarbons there needs to be made testing on cap rock leakage and cap rock threshold pressure to get a better understanding on the suitability of the structure. During the natural gas explorations focus was put on this structure, in the end it was deemed unusable as the last boreholes (Ky-5–Ky-7) showed no anticlinal structure to the north-east and it is highly unlikely that the structure is closed in this direction (Lindblom & Svenssson 1985). Therefore, further studies should not focus on this structure.

The Brown structure is less studied than the Green one, with no data on permeability, pressure, cap rock leakage and threshold pressure. There is a good chance that the permeability values are in the same range as for the Green structure since the lithology is quite similar. The pressure can, however, be considered lower as the structure is at a shallower depth. This could favour the structure. The volume of the Brown structure depends on how you utilize it. It is separated into two dome structures so it can either be seen as one structure or two smaller ones. If calculated together the volume is slightly smaller (0.88) than that of the largest planned CAES plant which would be excellent for large scale operation. If used as two separate structures they are only 0.3 and 0.2 times the size of the large CAES but 10 and 5 times the size of the smallest CAES in operation (the Huntorf plant in Germany). As no plant is planned in the area at the moment it is hard to evaluate the size needed, but to balance the power of the city of Lund large scale operation would be needed.

As with the Green structure the porosity is excellent, and it is the same type of reservoir (channel sandstones) that is good for CAES operations. There is the same uncertainty when it comes to hydrocarbons that might be on the high side, but still viewed as acceptable. The thickness of the cap rock is satisfactory for the Brown structure, but at only 2 m it is not optimal and was thought to be too thin at well Ky-4 for natural gas storage by Hagconsult AB (1983). The closure rating faces the same problems as for the Green structure where the average thickness of the reservoir gives a too low rating but with more knowledge of the exact thickness it might be usable if it thins out towards the edges of the structure. Focus should be on this structure for further investigations if the volume is deemed appropriate for CAES operation in the area.

The Lund Geothermal plant has been running for over 30 years and might need to be expanded or replaced in the future. Other parts of the Lund Sandstone distribution or deeper parts of the sandstone would be a good substitute as there are possibilities to find similar properties as in the Lund Geothermal Field. The results show slightly less sand in the top 200 m of the Lund Sandstone in the Kyrkheddinge area compared to the geothermal field. Three of the Kyrkheddinge wells, Ky-2, Ky-4 and Ky-7, show similar net sand as the production wells (>70%) which indicated a potential to be a good replacement area even though three of the other wells had much less net sand at around 40%. This shows how heterogenous the formation is, and more research would be needed to find the best placements for wells before a new plant is possible. In the Lund Geothermal Field the net sand over the filtered parts of the wells is 43–72 m for the production wells and 63–78 m for the injection wells with a net sand of around 69–83% and 50–58%, respectively. For economical purposes it is important with high net sand to keep well costs down and for better pumping results. It seems like this could be achieved in the Kyrkheddinge area but more spots with high net sand would need to be found to have a similar energy output as the existing geothermal plant.

It would be possible to have both CAES and geothermal operations in the area, as long as the geothermal wells do not penetrate the structure used for CAES operations. A geothermal plant would be a safer option with less research needed beforehand and a higher likelihood of success. CAES operations would have a higher upfront cost as more research would be needed beforehand, and it is a higher risk as the Brown structure that would be the possible target is not well researched and might not be possible to utilize.

Natural gas storage, hydrogen storage and CAES all have similar needs and would require similar

Fig. 17. Thin-section from well Ky-1 taken from a depth of 777 meters below sea level. It shows a possible reservoir layer with high porosity and a grain size at around 2–5 mm.

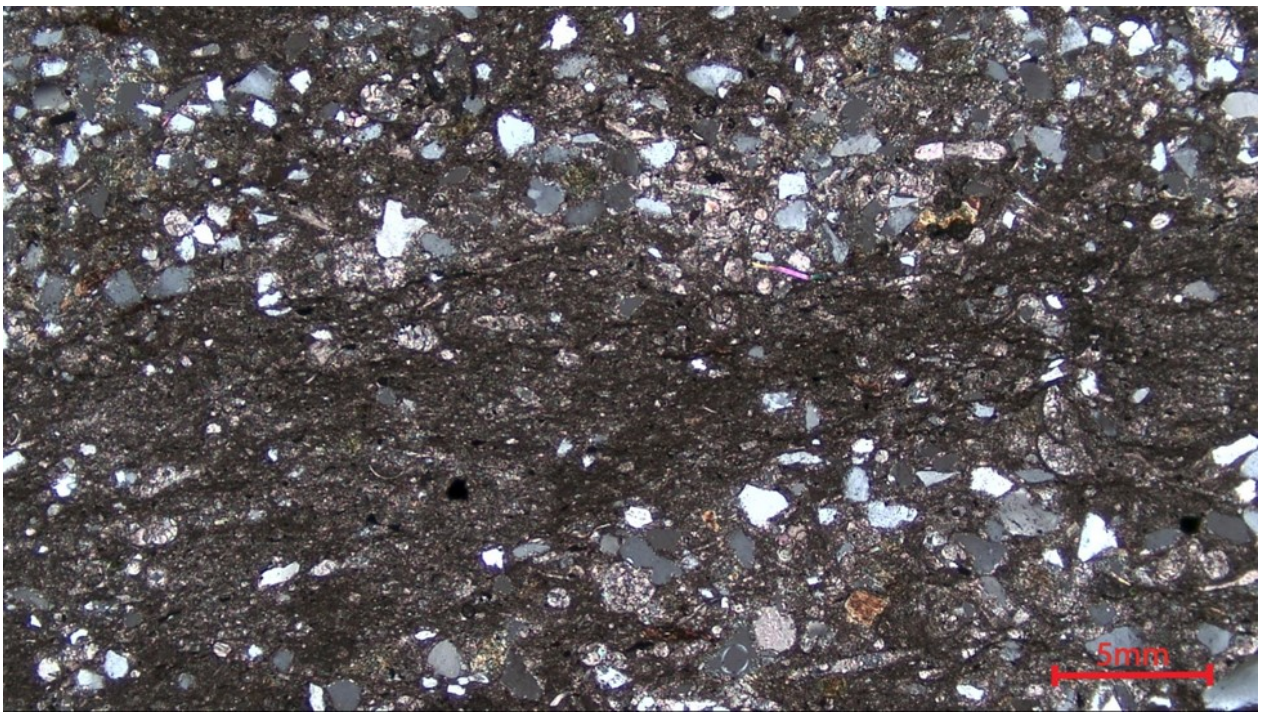

Fig. 18. Thin-section from well Ky-1 taken from a depth of 722 meters below sea level. It shows a potential caprock that is well cemented and fine grained with grain sizes <1 mm.

geological prerequisites. Hydrogen puts high demands on the caprock and the questionable caprock of the Brown Marker makes it not very likely it is going to work. Thermal energy storage could be a good option as it does not require a closed structure and could utilize the reservoir even if no closed structures are available. Underground pumped hydro would require excavation and is not the most efficient use of a porous aquifer.

8 Conclusion

Digitalizing analog isochron maps into a 3D model using ArcMap and ArcScene is not overly complex but time consuming. It is a good way to find and visualize closed structures. It can also be used to do precise calculations on the area and volume on these structures. It is not as useful for incorporating well data and making cross-sections, but it has been a useful asset in this

study. If the method is further developed and streamlined it could prove an important tool in similar studies.

The Kyrkheddinge area is likely a good place for geothermal energy utilization for district heating if expansion is needed for Lund and nearby towns. It would probably be the lowest risk and upfront cost geoenergy project in the area as geothermal energy is already utilized with success in the Lund Sandstone.
CAES could be possible in the Kyrkheddinge area. The Brown structure is the most likely option, but more research is needed. This is a more high-risk project with a higher upfront cost and the chance for success lower.

It would be possible to utilize both geothermal energy and have a CAES plant in the area as long as the geothermal energy does not use the structures used for CAES.

If no closed structure can be used, thermal energy could be the best option.

9 Acknowledgement

I want to thank my supervisor, Mikael Erlström, for all the help on the project. For helping me get started on the work in ArcMap I would like to thank Jonas Ising at SGU. I also want to thank all the other master students up at the fifth floor for the company and keeping me motivated. Most of all I want to thank Tove for always being there for me.

10 References

Aldenius, E., 2017: Lunds Geotermisystem, en utvärdering av 30 års drift. *Bachelor Thesis in Geology at the University of Lund*. 24 pp.

Allen, R., Doherty, T., Erikson, R. & Wiles, L., 1983. Factors affecting storage of compressed air in porous-rock reservoirs. *Pacific Northwest Lab* Report, Richland, WA (USA), 157 pp.

Alm, P.-G., 1999: Longtime Study of Geothermal Data from a Low Enthalpy Geothermal Heat Plant. *Twenty-Fourth Workshop on Geothermal Engineering.* Stanford University, California. 6 pp.

Alm, P.-G. & Bjelm, L., 1995: *Geothermal energy in Scania : a summary of research activities and results within the national program for geothermal energy in sedimentary rocks 1977-1994 : NUTEK Project 656 090-3*. Lund Institute of Technology, Dept. of Engineering Geology**.** 90 pp.

Andersson, J.-E., Carlsson, L. & Winberg, A., 1984. Preliminary groundwater model calculations in the Kyrkheddinge - Lund area. *SGAB* Report 40 pp.

Barbier, E., 2002: Geothermal energy technology and current status: An overview. *Renewable and Sustainable Energy Reviews 6***,** 3-65.

Barbier, M., Bondon, P., Mellinger, R. & Viallix, J. R., 1976: Mini-sosie for land seismology. *Geophysical Prospecting 24***,** 518-527.

Bertani, R., 2016: Geothermal power generation in the world 2010–2014 update report. *Geothermics 60***,** 31-43.

Bjelm, L., Erlström, M., Alm, P.-G., Rosberg, J.-E. & Ask, M., 2014. Infrastructure for Cap-rock Studies. *Division of Engingeering Geology, Lund University* Report, Swedish research council, 40 pp.

Bjelm, L. & Lindeberg, L., 1994: Long term experience from a heat pump plant in Lund, Sweden, using a low-temperature geothermal aquifer. *Conference on Geothermal Energy.* Milano. 4 pp.

Brown, A. & Eisentraut, A., 2014. Heating Without (Global) Warming. *International Energy Agency* Report 92 pp.

Cherns, L. & Larsson, K,. 1980. The Potential for Storage of Natural Gas in the Sedimentary Sequence of Scania. Phase 2, supplement. *Sveriges Geologiska Undersökning* Report 20 pp. 11 plates.

Epri-Doe, 2003. Handbook of Energy Storage for Transmission and Distribution Applications. *EPRI and the U.S. Department of Energy* Report 512 pp.

Erlström, M., 1990: *Petrology and deposition of the Lund Sandstone, Upper Cretaceous, southwestern Scania*. SGU Uppsala**.** 91 pp.

Erlström, M., 1994: Evolution of Cretaceous sedimentation in Scania. *Lund*, University of Lund. 36 pp.

Erlström, M., 2009. Tectonic evolution and geological framework of Scania – A review of interpretations and geological models. *Sveriges Geologiska Undersökning* Report 36 pp.

Erlström, M., 2017. The Lund Geothermal System - Background, Design, and Review of Operational Experiences. Geothermal project, Status report WP 3.2c and WP 5.1. *Lund University, Department of Geology.* Report 31 pp.

Erlström, M., Mellqvist, C., Schwartz, G., Gustafsson, M. & Dahlqvist, P., 2016. Geologisk Information för Geoenergianläggningar - en översikt. Report, Sveriges Geologiska Undersökningar, 56 pp.

European Commission, 2016: ESTMAP, Energy Stor age and Planning. Retrieved 2019-05-19, from www.estmap.eu.

Glassley, W. E., 2015: *Geothermal energy : renewable energy and the environment*. Boca Raton, Florida**.** 410 pp.

Hagconsult Ab, 1983. Progress Report No. 1 Aquifer Gas Storage at Kyrkheddinge. *Hagconsult AB* Report 72 pp.

Heward, A. P., 1981: A review of wave-dominated clastic shoreline deposits. *Earth-Science Reviews 17***,** 223-276.

Kumpas, M., 1981. The Potential for Storage of Natural Gas in the Sedimentary Sequence of Scania. Phase 3 Report Supplement. *Sverige Geologiska Undersökning* Report 10 pp.

Larsen, G., Christensen, O. B., Bang, I. & Busch, A., 1968. Öresund, Helsingør-Helsingborg Linien. Geologisk rapport. *Danmarks Geologiske Undersøgelse* Report 90 pp.

Larsson, K., 1982. Förutsättningarna för Lagring av Naturgas i Skånes Sedimentära Berggrund. Etapp 5. Delrapport 1: Kyrkheddinge. Sam-

manfattningar och Rekommendationer. *Sveriges Geologiska Undersökning* Report 14 pp. 5 plates.

Larsson, K. & Kumpas, M., 1982. the potential for storage of natural gas in the sedimentary sequence of scania. Phase 4 Report, Plates. *Sveriges Geologiska Undersökning* Report 19 pp.

Larsson, K., Solakius, N. & Vajda, V., 2000: Foraminifera and palynomorphs from the greensand-limestone sequences (Aptian-Coniacian) in southwestern Sweden. *Geologische Jahrbuch fur Geologie und Paläontologie 216*, 277-312.

Li, L., Weiguo, L., Haojie, L., Jianfeng, Y. & Maurice, D., 2018: Compressed air energy storage: characteristics, basic principles, and geological considerations. *Advances in Geo-Energy Research*, 135.

Lidmar-Bergström, K., 1982: *Pre-quaternary geomorphological evolution in southern Fennoscandia*. Lund. 202 pp.

Limberger, J., Boxem, T., Pluymaekers, M., Bruhn, D., Manzella, A., Calcagno, P., Beekman, F., Cloetingh, S. & Van Wees, J.-D., 2018: Geothermal energy in deep aquifers: A global assessment of the resource base for direct heat utilization. *Renewable and Sustainable Energy Reviews 82*, 961-975.

Lindblom, U. & Svenssson, L., 1985. Final Report, Aquifer Gas Storage at Kyrkheddinge. *Swedegas AB* Report 68 pp.

Lindström, S., Erlström, M., Boldreel, L., Kristensen, L., Nielsen, L., Mathiesen, A., Kamla, E. & Andersen, M. S., 2018: Stratigraphy and geothermal assessment of Mesozoic sandstone reservoirs in the Øresund Basin – exemplified by well data and seismic profiles. *Bulletin of the Geological Sociaty of Denmark 66*, 123-149.

Lord, A. S., 2009. Overview of geologic storage of natural gas with an emphasis on assessing the feasibility of storing hydrogen. *Sandia National Laboratory* Report 28 pp.

Lund, J. W. & Boyd, T. L., 2016: Direct utilization of geothermal energy 2015 worldwide review. *Geothermics 60*, 66-93.

Lunds Tekniska Högskola, 1984. Slutrapport EFN - Projekt 41113 012 Geoprov Lund, Tester, dokumentation och utvärdering av det geotermiska projektet i Lund., *Lunds Tekniska Högskola* Report, Lund, 45 pp.

Mouli-Castillo, J., Wilkinson, M., Mignard, D., Mcdermott, C., Haszeldine, R. S. & Shipton, Z., 2019: Inter-seasonal compressed-air energy storage using saline aquifers. *Nature Energy 4*, 9.

Muttaqi, K. M., Islam, M. R. & Sutanto, D., 2019: Future Power Distribution Grids: Integration of Renewable Energy, Energy Storage, Electric Vehicles, Superconductor, and Magnetic Bus. *IEEE Transactions on Applied Superconductivity*, 5.

Norling, E., 1981: Upper Jurassic and Lower Cretaceous geology of Sweden. *GFF 103*, 253-269.

Pegrum, R. M., 1984: The extension of the Tornquist Zone in the Norwegian North Sea. *Norsk Geologisk Tidsskrift 64*, 39-68.

Pickard, W. F., 2012: The History, Present State, and Future Prospects of Underground Pumped Hydro for Massive Energy Storage. *Proceedings of the IEEE*, 473-483.

PLE, 1983. Natural gas aquifer storage field. Kyrkheddinge seismic report. *Pipeline Engineering* Report. 7 pp. 29 plates.

Rudolph, H., Zhou, Y., Song, P., Zhang, Y. & Lei, X., 2018: Aquifer Thermal Energy Storage in the Netherlands: A Review. *2018 International Conference on Power System Technology (POWERCON).* 545-552 pp.

Sainz-Garcia, A., Abarca, E., Rubi, V. & Grandia, F., 2017: Assessment of feasible strategies for seasonal underground hydrogen storage in a saline aquifer. *International Journal of Hydrogen Energy 42*, 16657-16666.

Schmidt, T., Pauschinger, T., Sørensen, P. A., Snijders, A., Djebbar, R., Boulter, R. & Thornton, J., 2018: Design Aspects for Large-scale Pit and Aquifer Thermal Energy Storage for District Heating and Cooling. *Energy Procedia 149*, 585-594.

SGU, 1981. The Potential for Storage of Natural Gas in the Sedimentary Sequence of Scania. Phase 3 report. Suppliment, Plates. *Sveriges Geologiska Undersökning* Report.

Shatnawi, M., Qaydi, N. A., Aljaberi, N. & Aljaberi, M., 2018: Hydrogen-Based Energy Storage Systems: A Review. *2018 7th International Conference on Renewable Energy Research and Applications (ICRERA).* 697-700 pp.

Sivhed, U., Erlström, M. & Wikman, H., 1999: *Beskrivning till berggrundskartorna 1C Trelleborg NV och NO samt 2C Malmö SV, SO, NV och NO: Description to the maps of solid rocks Trellborg NV and NO, Malmö SV, SO, NV and NO*. Sveriges Geologiska Undersökning. 143 pp.

Sofregaz, 1982. Interpretation report of the Kyrkheddinge seismic survey, May—June 1982. *Compagnie Generale de Geophysique* Report. 8 pp. 8 figs. 4 plates.

Sopher, D., Juhlin, C., Levendal, T., Erlström, M. & Nilsson, K., 2019: Evaluation of the subsurface compressed air energy storage (CAES) potential on Gotland, Sweden. *Environmental Earth Sciences 78*, 17.

Stefansson, V., 2005: World geothermal assessment. *Proceedings world geothermal congress.* 24-29 pp.

Succar, S. & Williams, R. H., 2008: *Compressed air energy storage: theory, resources, and applications for wind power*. Princeton Environmental Institute. 81 pp.

Tyson, R. V. & Funnell, B. M., 1987: European cretaceous shorelines, stage by stage. *Palaeogeography, Palaeoclimatology, Palaeoecology 59*, 69-91.

Uddin, N., 2012: Geotechnical Issues in the Creation of Underground Reservoirs for Massive Ener-

gy Storage. *Proceedings of the IEEE*, 484-492.
Venkataramani, G., Parankusam, P., Ramalingam, V. & Wang, J., 2016: A review on compressed air energy storage – A pathway for smart grid and polygeneration. *Renewable and Sustainable Energy Reviews 62*, 895-907.
Wang, Z., Wang, J., Lan, C., He, I., Ko, V., Ryan, D. & Wigston, A., 2016: A study on the impact of SO2 on CO2 injectivity for CO2 storage in a Canadian saline aquifer. *Applied Energy 184*, 329-336.

Appendix

Appendix 1. Isochron map showing the depth of the Tan Marker in the Kyrkheddinge area (Larsson 1982).

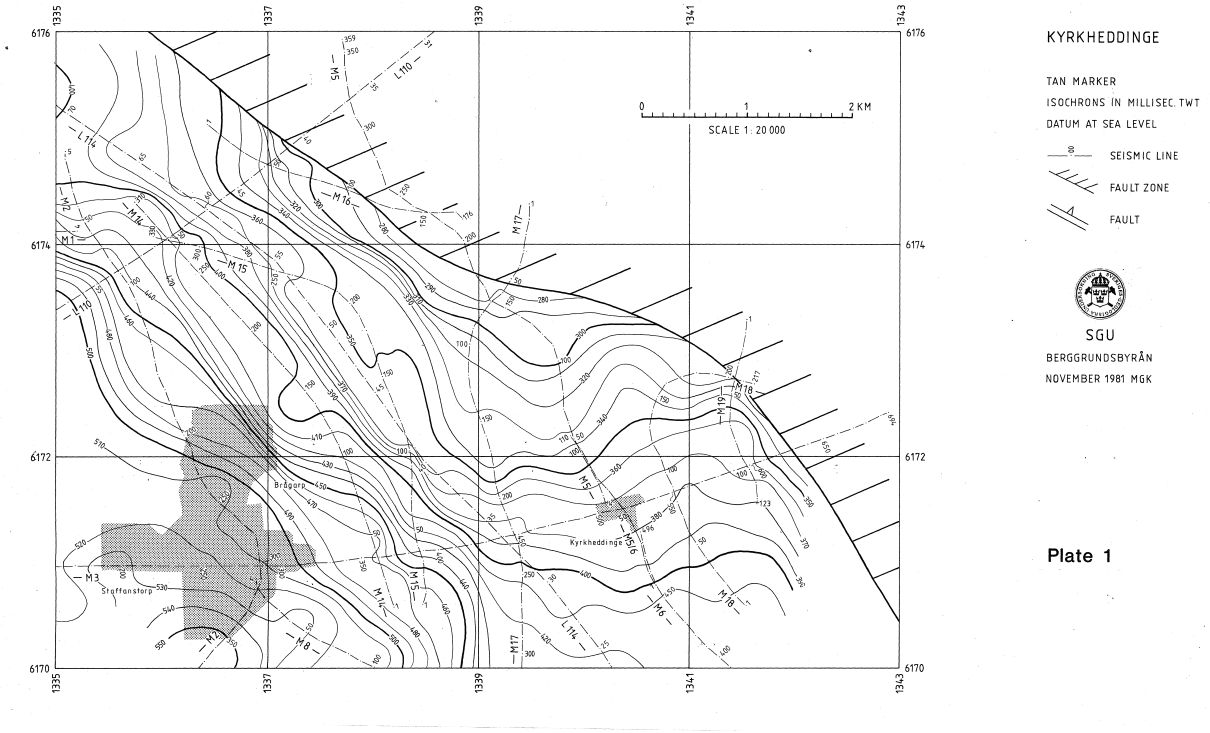

Appendix 2. Isochron map showing the depth of the Orange Marker in the Lund-Mossheddinge area (SGU 1981).

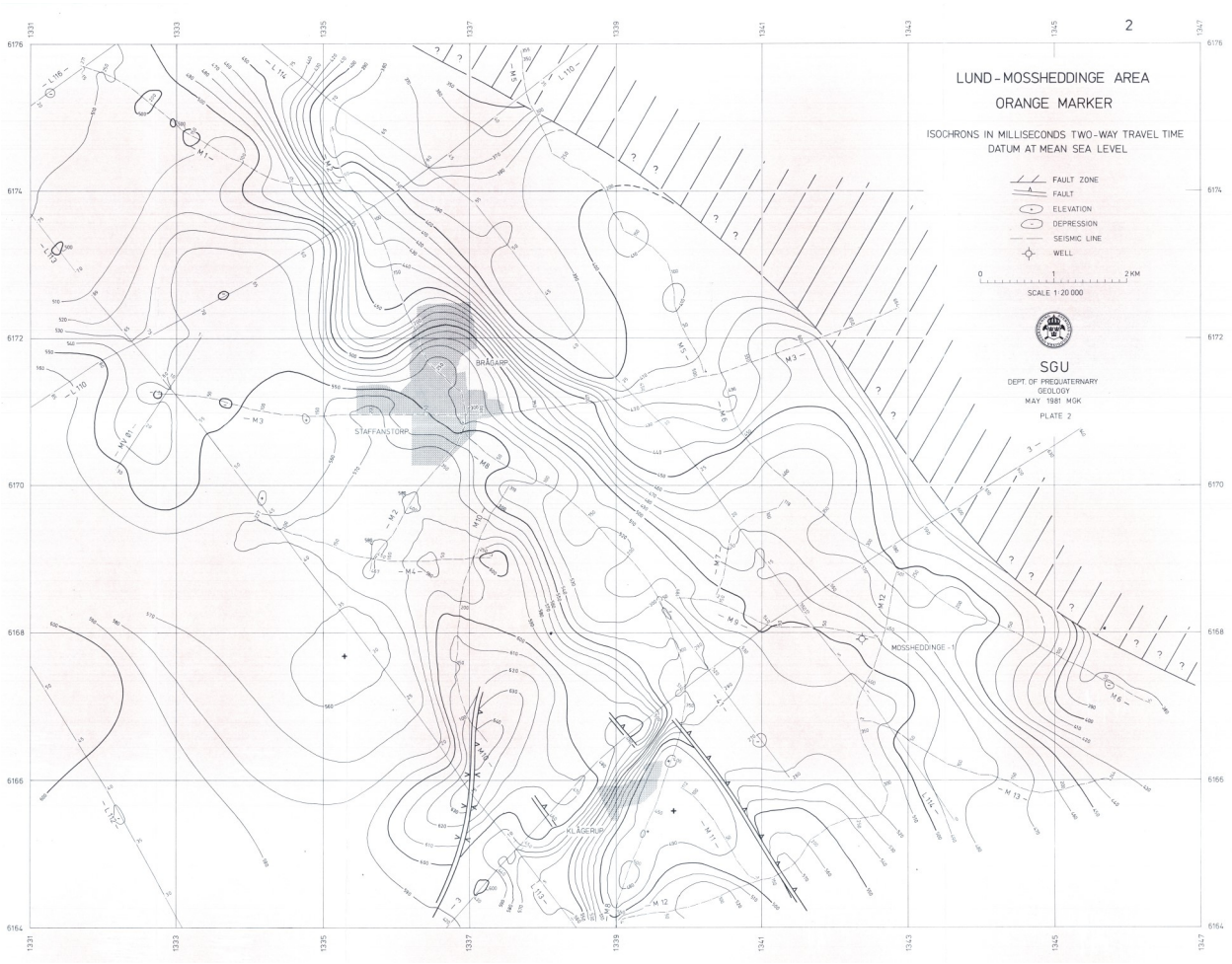

Appendix 3. Isochron map showing the depth of the Orange Marker in the Mossheddinge-Sturup area (Larsson & Kumpas 1982).

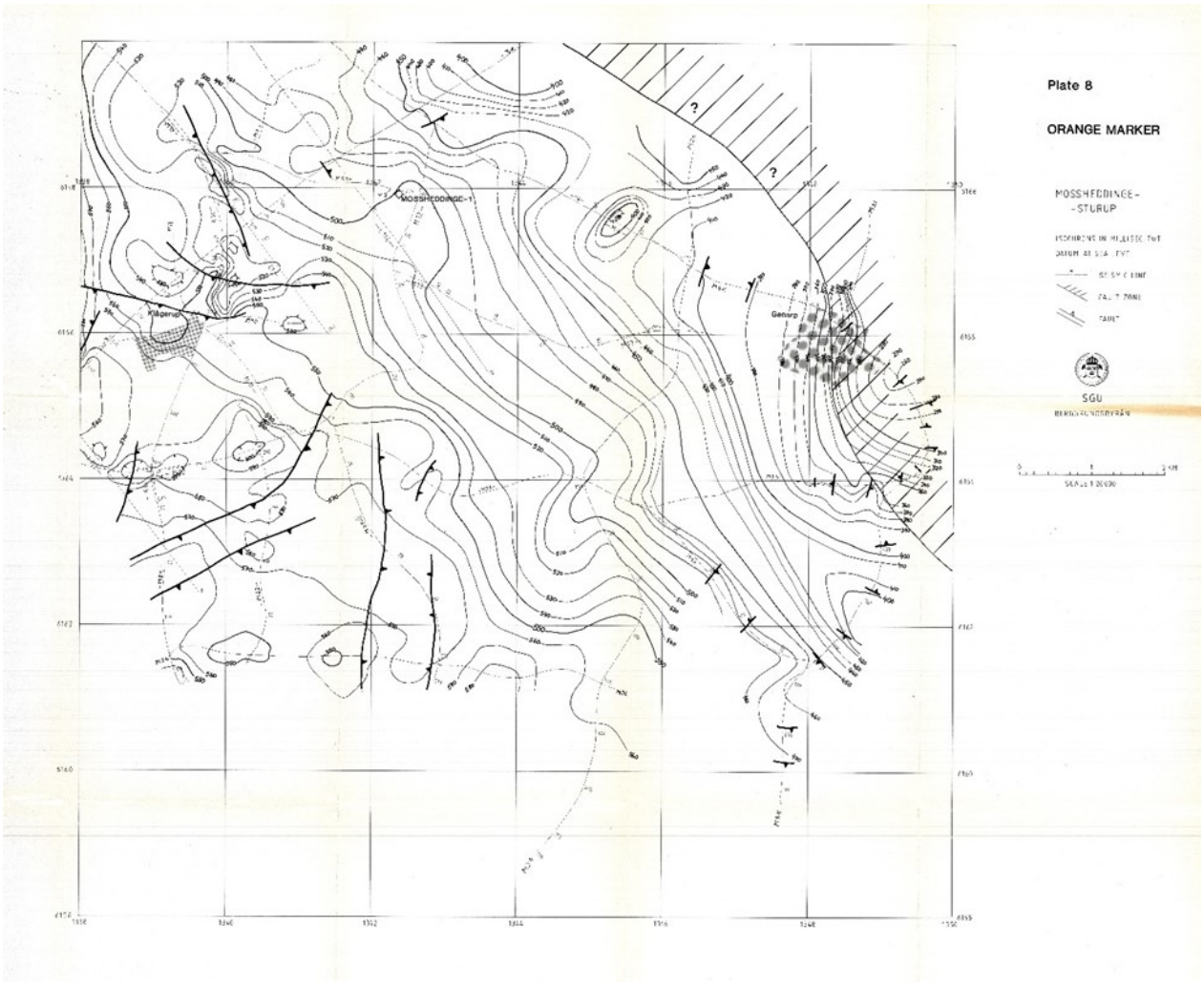

Appendix 4. Isochron map showing the depth of the Orange Marker in south-western Skåne (SGU 1981)

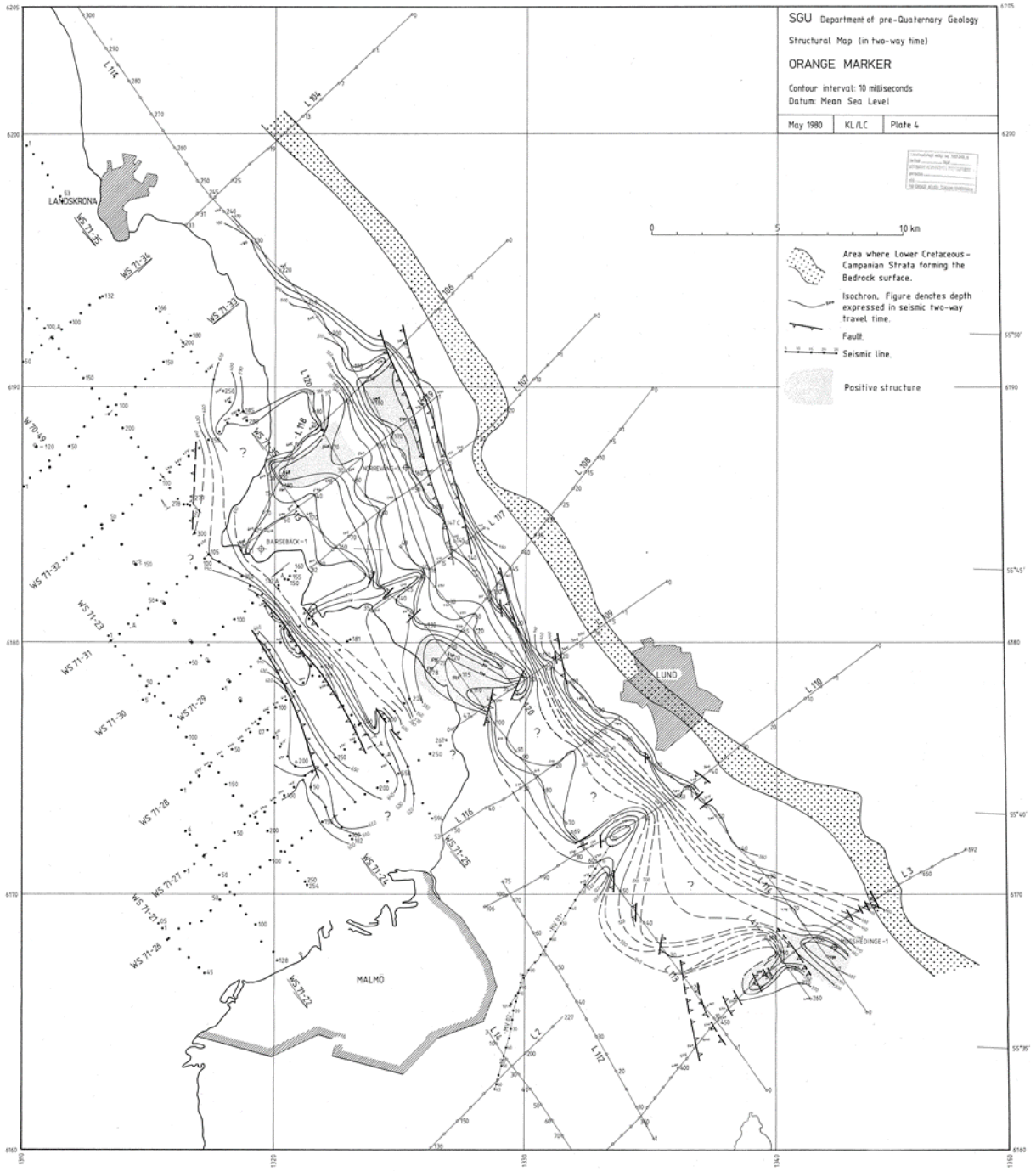

Appendix 5. Isochron map showing the depth of the Brown Marker in the Lund-Mossheddinge area (SGU 1981)

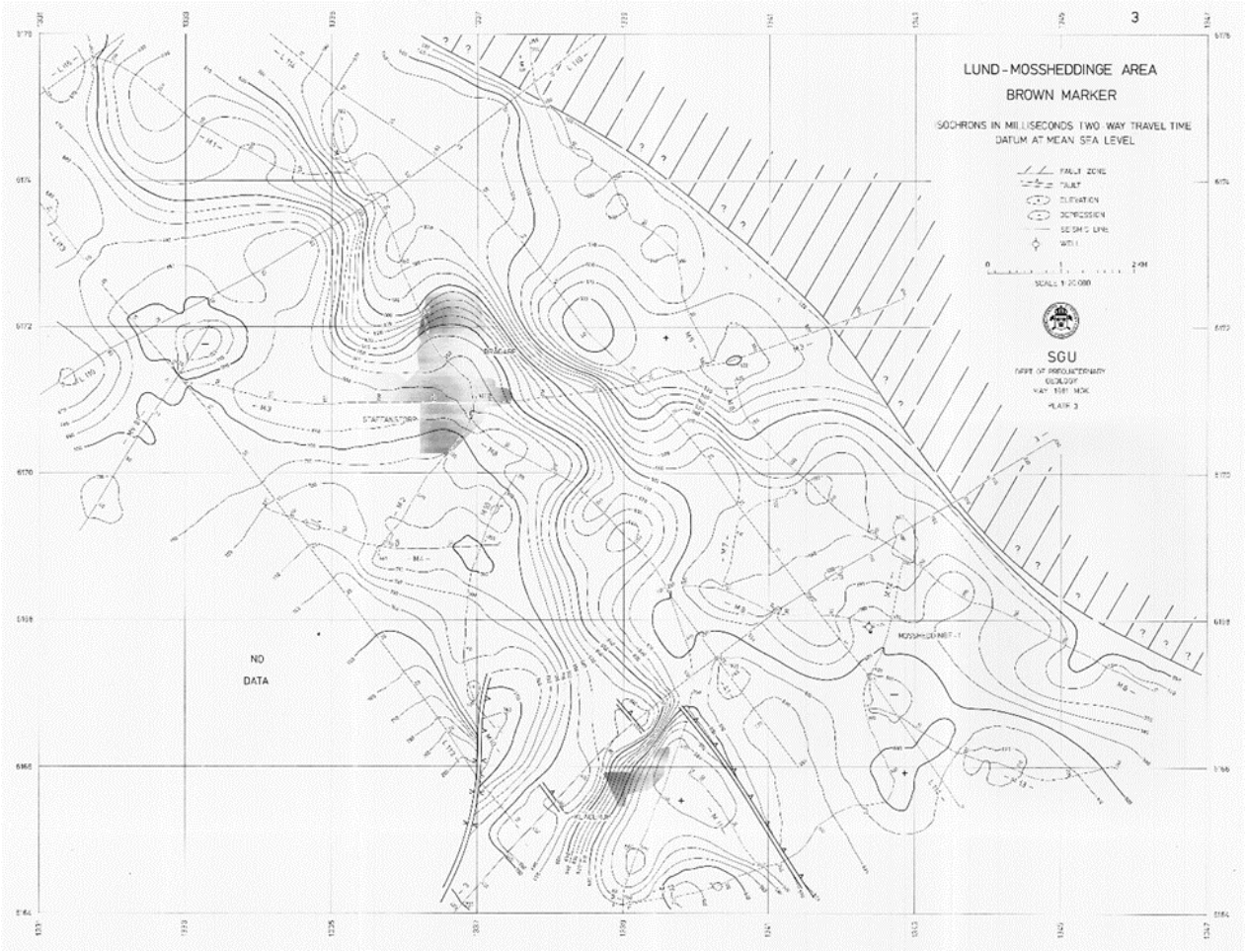

Appendix 6. Isochron map showing the depth of the Brown Marker in the Mossheddinge-Sturup area (Larsson & Kumpas 1982).

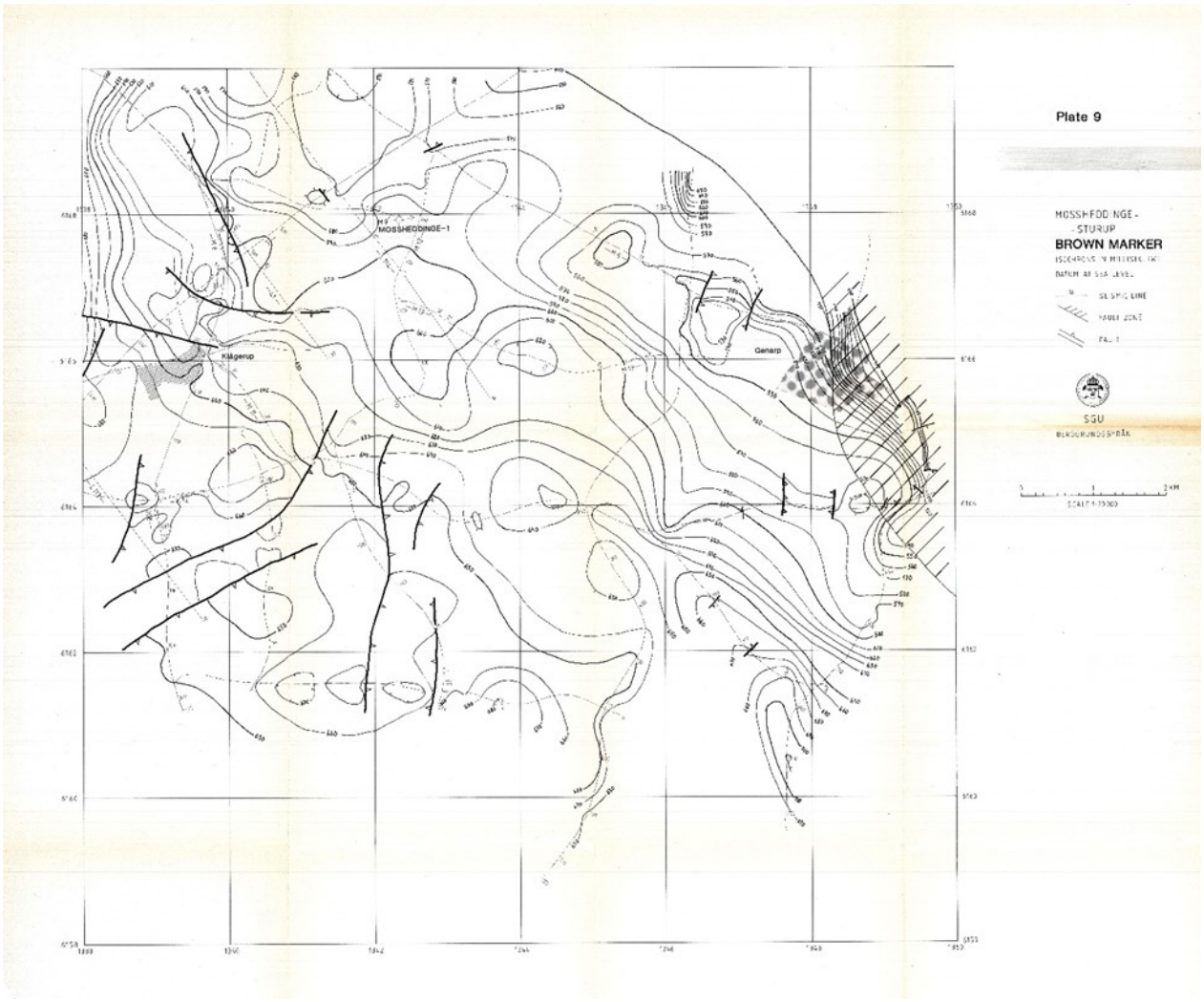

Appendix 7. Isochron map showing the depth of the Yellow Marker in the Lund-Mossheddinge area (SGU 1981)

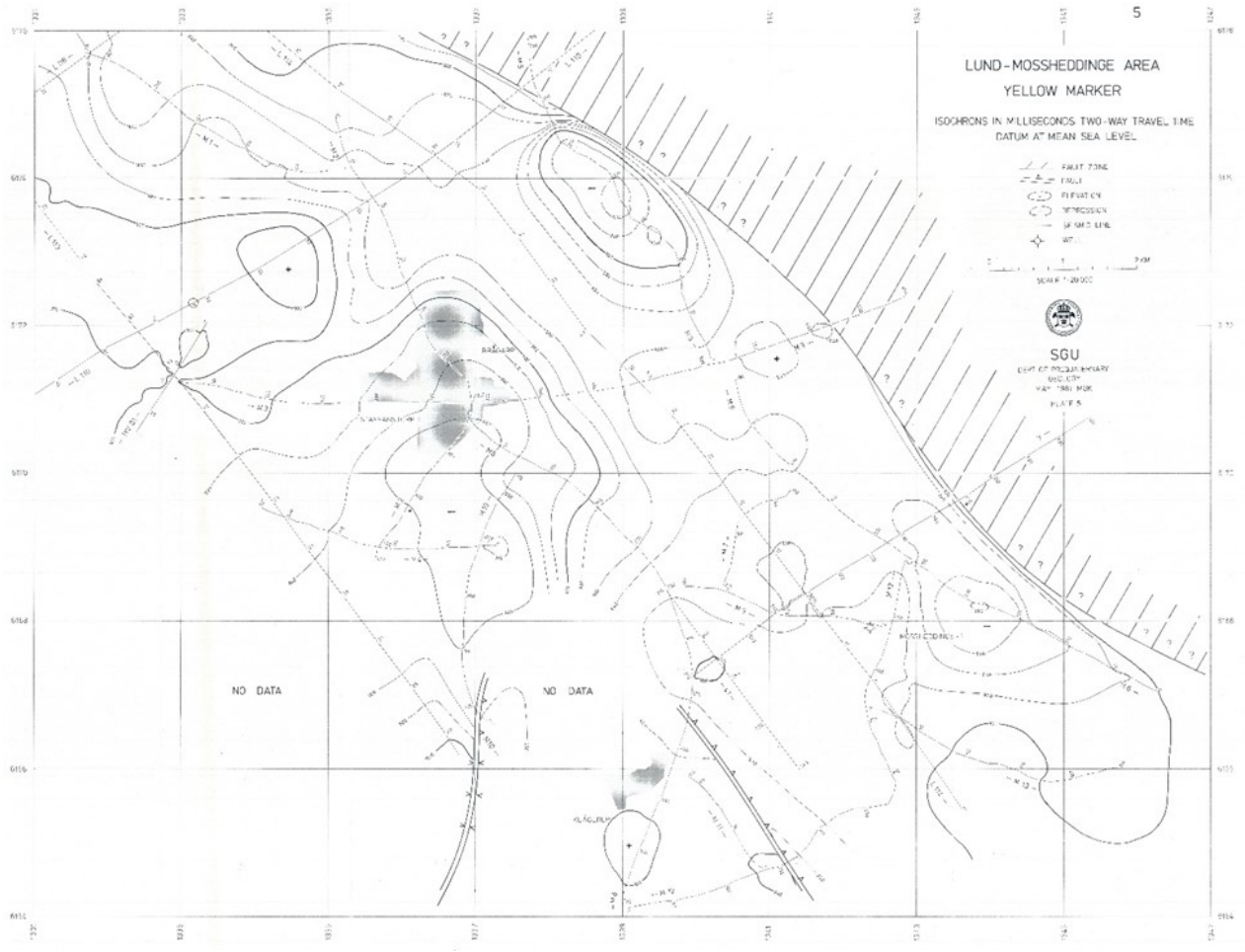

Appendix 8. Isochron map showing the depth of the Yellow Marker in south-western Skåne (SGU 1981)

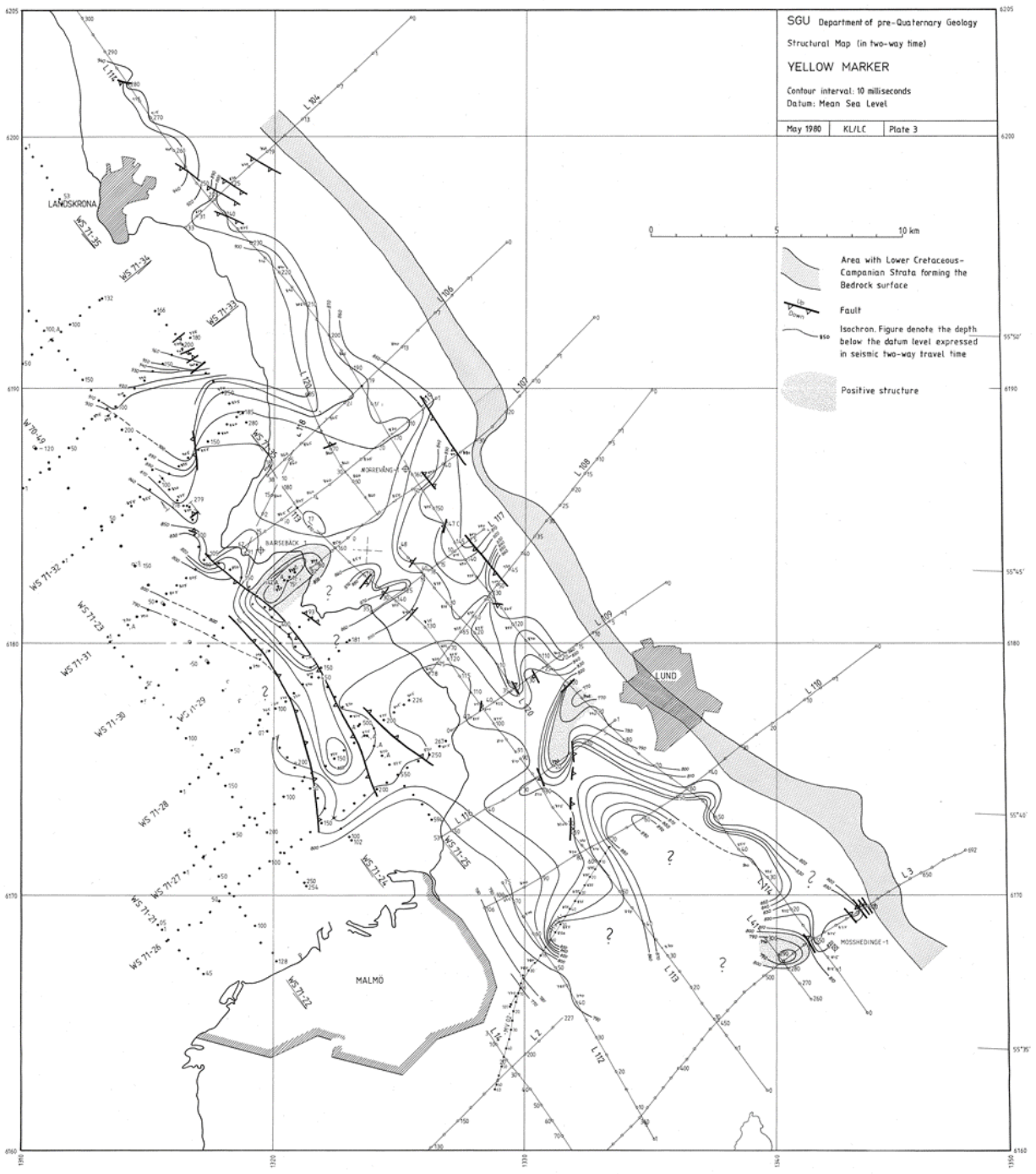

Tidigare skrifter i serien ”Examensarbeten i Geologi vid Lunds universitet”:

517. Hydén, Christina Engberg, 2017: Drumlinerna i Löberöd - Spår efter flera isrörelseriktningar i mellersta Skåne. (15 hp)
518. Svantesson, Fredrik, 2017: Metodik för kartläggning och klassificering av erosion och släntstabilitet i vattendrag. (45 hp)
519. Stjern, Rebecka, 2017: Hur påverkas luminiscenssignaler från kvarts under laboratorieförhållanden? (15 hp)
520. Karlstedt, Filippa, 2017: P-T estimation of the metamorphism of gabbro to garnet amphibolite at Herrestad, Eastern Segment of the Sveconorwegian orogen. (45 hp)
521. Önnervik, Oscar, 2017: Ooider som naturliga arkiv för förändringar i havens geokemi och jordens klimat. (15 hp)
522. Nilsson, Hanna, 2017: Kartläggning av sand och naturgrus med hjälp av resistivitetsmätning på Själland, Danmark. (15 hp)
523. Christensson, Lisa, 2017: Geofysisk undersökning av grundvattenskydd för planerad reservvattentäkt i Mjölkalånga, Hässleholms kommun. (15 hp)
524. Stamsnijder, Joaen, 2017: New geochronological constraints on the Klipriviersberg Group: defining a new Neoarchean large igneous province on the Kaapvaal Craton, South Africa. (45 hp)
525. Becker Jensen, Amanda, 2017: Den eocena Furformationen i Danmark: exceptionella bevaringstillstånd har bidragit till att djurs mjukdelar fossiliserats.(15 hp)
526. Radomski, Jan, 2018: Carbonate sedimentology and carbon isotope stratigraphy of the Tallbacken-1 core, early Wenlock Slite Group, Gotland, Sweden. (45 hp)
527. Pettersson, Johan, 2018: Ultrastructure and biomolecular composition of sea turtle epidermal remains from the Campanian (Upper Cretaceous) North Sulphur River of Texas. (45 hp)
528. Jansson, Robin, 2018: Multidisciplinary perspective on a natural attenuation zone in a PCE contaminated aquifer. (45 hp)
529. Larsson, Alfred, 2018: Rb-Sr sphalerite data and implications for the source and timing of Pb-Zn deposits at the Caledonian margin in Sweden. (45 hp)
530. Balija, Fisnik, 2018: Stratigraphy and pyrite geochemistry of the Lower–Upper Ordovician in the Lerhamn and Fågelsång -3 drill cores, Scania, Sweden. (45 hp)
531. Höglund, Nikolas, 2018: Groundwater chemistry evaluation and a GIS-based approach for determining groundwater potential in Mörbylånga, Sweden. (45 hp)
532. Haag, Vendela, 2018: Studie av mikrostrukturer i karbonatslagkäglor från nedslagsstrukturen Charlevoix, Kanada. (15 hp)
533. Hebrard, Benoit, 2018: Antropocen – vad, när och hur? (15 hp)
534. Jancsak, Nathalie, 2018: Åtgärder mot kusterosion i Skåne, samt en fallstudie av erosionsskydden i Löderup, Ystad kommun. (15 hp)
535. Zachén, Gabriel, 2018: Mesosideriter – redogörelse av bildningsprocesser samt SEM-analys av Vaca Muertameteoriten. (15 hp)
536. Fägersten, Andreas, 2018: Lateral variability in the quantification of calcareous nannofossils in the Upper Triassic, Austria. (15 hp)
537. Hjertman, Anna, 2018: Förutsättningar för djupinfiltration av ytvatten från Ivösjön till Kristianstadbassängen. (15 hp)
538. Lagerstam, Clarence, 2018: Varför svalde svanödlor (Reptilia, Plesiosauria) stenar? (15 hp)
539. Pilser, Hannes, 2018: Mg/Ca i bottenlevande foraminiferer, särskilt med avseende på temperaturer nära 0°C. (15 hp)
540. Christiansen, Emma, 2018: Mikroplast på och i havsbotten - Utbredningen av mikroplaster i marina bottensediment och dess påverkan på marina miljöer. (15 hp)
541. Staahlnacke, Simon, 2018: En sammanställning av norra Skånes prekambriska berggrund. (15 hp)
542. Martell, Josefin, 2018: Shock metamorphic features in zircon grains from the Mien impact structure - clues to conditions during impact. (45 hp)
543. Chitindingu, Tawonga, 2018: Petrological characterization of the Cambrian sandstone reservoirs in the Baltic Basin, Sweden. (45 hp)
544. Chonewicz, Julia, 2018: Dimensionerande vattenförbrukning och alternativa vattenkvaliteter. (15 hp)
545. Adeen, Lina, 2018: Hur lämpliga är de geofysiska metoderna resistivitet och IP för kartläggning av PFOS? (15 hp)
546. Nilsson Brunlid, Anette, 2018: Impact of southern Baltic sea-level changes on landscape development in the Verkeån River valley at Haväng, southern Sweden, during the early and mid Holocene. (45 hp)
547. Perälä, Jesper, 2018: Dynamic Recrystallization in the Sveconorwegian Frontal Wedge, Småland, southern Sweden. (45 hp)
548. Artursson, Christopher, 2018: Stratigra-

phy, sedimentology and geophysical assessment of the early Silurian Halla and Klinteberg formations, Altajme core, Gotland, Sweden. (45 hp)

549. Kempengren, Henrik, 2018: Att välja den mest hållbara efterbehandlingsmetoden vid sanering: Applicering av beslutsstödsverktyget SAMLA. (45 hp)
550. Andreasson, Dagnija, 2018: Assessment of using liquidity index for the approximation of undrained shear strength of clay tills in Scania. (45 hp)
551. Ahrenstedt, Viktor, 2018: The Neoproterozoic Visingsö Group of southern Sweden: Lithology, sequence stratigraphy and provenance of the Middle Formation. (45 hp)
552. Berglund, Marie, 2018: Basaltkuppen - ett spel om mineralogi och petrologi. (15 hp)
553. Hernnäs, Tove, 2018: Garnet amphibolite in the internal Eastern Segment, Sveconorwegian Province: monitors of metamorphic recrystallization at high temperature and pressure during Sveconorwegian orogeny. (45 hp)
554. Halling, Jenny, 2019: Characterization of black rust in reinforced concrete structures: analyses of field samples from southern Sweden. (45 hp)
555. Stevic, Marijana, 2019: Stratigraphy and dating of a lake sediment record from Lyngsjön, eastern Scania - human impact and aeolian sand deposition during the last millennium. (45 hp)
556. Rabanser, Monika, 2019: Processes of Lateral Moraine Formation at a Debris-covered Glacier, Suldenferner (Vedretta di Solda), Italy. (45 hp)
557. Nilsson, Hanna, 2019: Records of environmental change and sedimentation processes over the last century in a Baltic coastal inlet. (45 hp)
558. Ingered, Mimmi, 2019: Zircon U-Pb constraints on the timing of Sveconorwegian migmatite formation in the Western and Median Segments of the Idefjorden terrane, SW Sweden. (45 hp)
559. Hjorth, Ingeborg, 2019: Paleomagnetisk undersökning av vulkanen Rangitoto, Nya Zeeland, för att bestämma dess utbrottshistoria. (15 hp)
560. Westberg, Märta, 2019: Enigmatic worm-like fossils from the Silurian Waukesha Lagerstätte, Wisconsin, USA. (15 hp)
561. Björn, Julia, 2019: Undersökning av påverkan på hydraulisk konduktivitet i förorenat område efter in situ-saneringsförsök. (15 hp)
562. Faraj, Haider, 2019: Tolkning av georadarprofiler över grundvattenmagasinet Verveln - Gullringen i Kalmar län. (15 hp)
563. Bjermo, Tim, 2019: Eoliska avlagringar och vindriktningar under holocen i och kring Store Mosse, södra Sverige. (15 hp)
564. Langkjaer, Henrik, 2019: Analys av Östergötlands kommande grundvattenresurser ur ett klimtperspektiv - med fokus på förstärkt grundvattenbildning. (15 hp)
565. Johansson, Marcus, 2019: Hur öppet var landskapet i södra Sverige under Atlantisk tid? (15 hp)
566. Molin, Emmy, 2019: Litologi, sedimentologi och kolisotopstratigrafi över krita–paleogen-gränsintervallet i borrningen Limhamn-2018. (15 hp)
567. Schroeder, Mimmi, 2019: The history of European hemp cultivation. (15 hp)
568. Damber, Maja, 2019: Granens invandring i sydvästa Sverige, belyst genom pollenanalys från Skottenesjön. (15 hp)
569. Lundgren Sassner, Lykke, 2019: Strandmorfologi, stranderosion och stranddeposition, med en fallstudie på Tylösand sandstrand, Halland. (15 hp)
570. Greiff, Johannes, 2019: Mesozoiska konglomerat och Skånes tektoniska utveckling. (15 hp)
571. Persson, Eric, 2019: An Enigmatic Cerapodian Dentary from the Cretaceous of southern Sweden. (15 hp)
572. Aldenius, Erik, 2019: Subsurface characterization of the Lund Sandstone – 3D model of the sandstone reservoir and evaluation of the geoenergy storage potential, SW Skåne, South Sweden. (45 hp)

LUNDS UNIVERSITET

Geologiska institutionen
Lunds universitet
Sölvegatan 12, 223 62 Lund